The cytosolic role of EZH2-IMPDH2 complex in melanoma progression and metastasis via GTP regulation

*Gamze Kuser-Abali1, Fumihito Noguchi1, Pacman Szeto1,3, Youfang Zhang1,3, Cheng Huang2, Christopher K. Barlow2, Giovanna Pomilio1, Christopher Chew1, Samar Masoumi Moghaddam1, Peinan Zhao1, Miles Andrews1,3, Isobel Leece1, Jen G. Cheung1,3, Malaka Ameratunga1,3, Nicholas C. Wong1,4, Ralf B. Schittenhelm2, Andrew Wei1,3, Mark Shackleton1,3**

1. Central Clinical School, Monash University, Melbourne, Victoria, Australia
2. Monash Proteomics and Metabolomics Facility and the Department of Biochemistry and Molecular Biology, Biomedicine Discovery Institute, Monash University, Clayton, VIC 3800, Australia.
3. Alfred Health, Melbourne, Victoria, Australia
4. Monash Bioinformatics Platform, Monash University, Melbourne, Victoria, Australia

***To whom correspondence should be addressed:**

Mark Shackleton

Alfred Health

55 Commercial Road

Melbourne VIC, 3004Australia

E-mail: mark.shackleton@monash.edu

Highlights

- EZH2 has non-canonical methyltransferase independent, but GTP-dependent tumorigenic and metastatic function in melanoma.
- The N-terminal EED-binding domain of cytosolic EZH2 interacts with the CBS domain of IMPDH2 in a polycomb repressive complex 2- (PRC2-) and methylation-independent manner in a range of cancers including melanoma.

- Cytosolic EZH2 accumulates IMPDH2 in the cytoplasm and increases its tetramerization independent of its methyltransferase activity.
- EZH2 upregulates GTP synthesis by IMPDH2 and thereby activates ribosome biogenesis via rRNA synthesis. In parallel, EZH2 upregulates actomyosin contractility via RhoA GTPase activation.
- Sappanone A (SA) inhibits the IMPDH2-EZH2 interaction and is anti-proliferative across a range of cancers including melanoma, but not in normal melanocytes and bone marrow progenitor cells.

Graphical Abstract

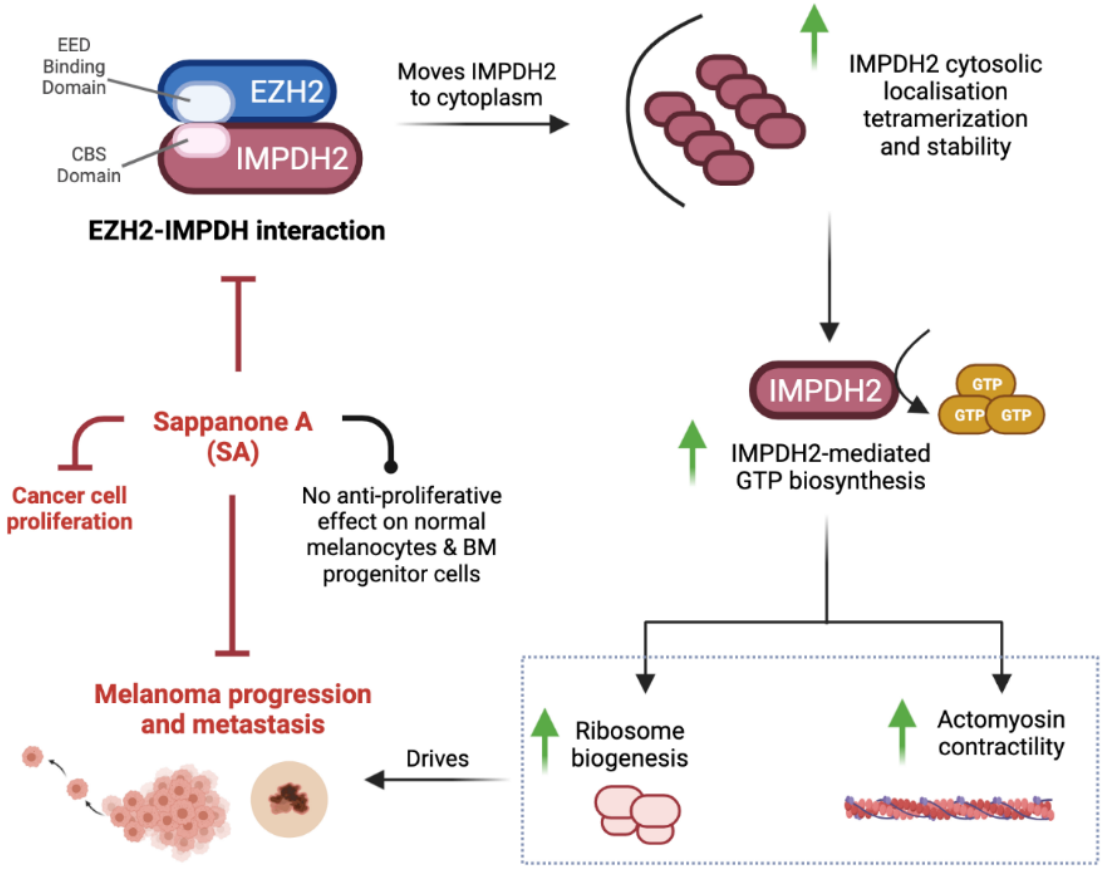

SUMMARY

Although conventional EZH2 enzymatic inhibitors have shown preclinical efficacy in various tumors, here we demonstrated that B-Raf mutant melanoma cells do not

respond effectively to pharmacological inhibition of EZH2 *in vitro*. Based on our LC-MS and biochemical assays, N-terminal of cytosolic EZH2 interacts with IMPDH2 through the IMPDH2-CBS domain in a PRC2- and methylation-independent (MTI) manner. Cytosolic EZH2 induces cytosolic accumulation of IMPDH2 and increases its tetramerization (activity). EZH2 upregulates cellular GTP levels via IMPDH2 activation and guanosine rescues siEZH2-reduced clonogenicity/invasion phenotype by regulating rRNA metabolism and Rho GTPase activity. Sappanone A by reducing the EZH2/IMPDH2 interaction and IMPDH2 tetramerization attenuates the growth/ invasion abilities of a range of cancers including, cutaneous / uveal melanoma, breast, prostate, ovarian cancer *in vitro,* but has no cytotoxic effect on melanocytes or bone marrow progenitor cells. These results point to a MTI, but GTP-mediated non-canonical mechanism of EZH2 in melanoma progression and metastasis.

Keywords: EZH2, IMPDH2, melanoma, Sappanone A, ribosome biogenesis, actomyosin contractility, GTP metabolism

INTRODUCTION

Neoplastic cells, including melanoma, are highly dependent on *de novo* biosynthesis of purine nucleotides [1]. Cellular GTP levels, critical for purine nucleotide synthesis, are significantly higher in melanoma cells when compared to melanocytes [2]. Melanoma cells regulate the activity of several Rho-GTPases involved in cell invasion via small alterations of intracellular GTP pools [2]. Rho-GTPases regulate the formation of the actomyosin cytoskeleton, thereby influencing adhesion, migration, and invasion in various cancers including melanoma [3,4].

Increased rRNA synthesis [5] and nucleolar hypertrophy [6] have both long been recognized as features of malignant transformation. The requirement of GTP for Pol I transcription and nucleolar hypertrophy has been shown recently in glioblastoma [7]. Previous studies showed that nucleolar hypertrophy was associated with thicker and more mitotically active melanoma tumors [8]. Selective inhibition of rRNA synthesis using the RNA polymerase I inhibitor CX-5461 decreased melanoma tumorigenicity *in vitro* and *in vivo* [9].

Inosine monophosphate dehydrogenase 2 (IMPDH2), an oncogene in various cancers [10] is a key rate-limiting enzyme in nucleotide synthesis, maintaining GTP

levels needed for nucleic acid synthesis, protein synthesis via ribosome biogenesis, and molecular signaling through the family of guanine nucleotide-binding proteins (G-proteins) that regulate numerous cell functions, such as cytoskeletal rearrangements, membrane traffic, protein synthesis and signal transduction [11]. IMPDH2 is regulated transcriptionally, post-translationally, and allosterically [12]. Tetramerization of IMPDH2 is essential for its activity [13,14]. IMPDH2 contains two major domains: the catalytic domain for substrate interaction and the Bateman domain (CBS), which is not required for catalytic activity but exerts an important allosteric regulation effect on IMPDH2 activity by communicating with the catalytic domain [13,15]. [16] reported that a naturally occurring compound, Sappanone A (SA), demonstrated significant inhibitory effects on neuroinflammation by directly targeting the conserved cysteine residue 140 (Cys140) in the CBS domain of IMPDH2. Interestingly, SA selectively targets and inactivates IMPDH2 but not IMPDH1, which eliminated apparent hematological side effects [16]. IMPDH2 is overexpressed in melanoma cell lines compared to melanocytes [17,18]. Notably, depletion of GTP via IMPDH2 inhibition with mycophenolate (MPA) induces cellular differentiation in melanoma cells [19].

Enhancer of zeste homolog 2 (EZH2), a component of Polycomb Repressor Complex 2 (PRC2), catalyzes tri-methylation of histone H3 at lysine 27 (H3K27me3) to regulate gene expression [20-22]. It has critical roles in the progression of numerous malignancies[23], including melanoma [24-28]. Recently, it has been shown that EZH2 activation in melanoma represses transcriptional genes associated with tumor suppression, cell differentiation, cell cycle inhibition, repression of metastasis, and antigen processing and presentation pathways [27-30]. EZH2 methyl-transferase inhibitors have shown anti-cancer activity preclinically [31,32] and in patients [31,33] with higher toxicity. Additional to methyl-transferase activity, EZH2 also interacts with transcription factors in PRC2- and methylation-independent that limit the therapeutic potential of EZH2 methyl-transferase inhibitors [34]. Compounds that degrade total EZH2 protein or that target methyltransferase-independent mechanisms of EZH2 might be required to avail the context-dependent therapeutic potential of EZH2 targeting. We have recently demonstrated that EZH2 is a negative regulator of melanocytic differentiation (pigmentation), whose suppression by knockdown or degraders decreased low pigmented melanoma cell clonogenicity and invasion and induced pigmentation [35]. However, conventional enzymatic inhibitors were less effective *in vitro* [35]. Overall, these data hinted that EZH2 has methyltransferase-

independent, non-catalytic function(s) in melanoma tumorigenesis and invasion, prompting us to look for novel EZH2 interactions in melanoma cells.

Although EZH2 is mainly intranuclear, some studies have shown its cytosolic localization in fibroblasts, T lymphocytes, breast cancer, and prostate cancer cells [36-39]. Studies have mostly focused on the nuclear functions of EZH2, and the functions of EZH2 in the cytoplasm have remained elusive.

EZH2 can influence the development and progression of tumors by facilitating glucose, lipid, and amino acid metabolism [40,41] However, no evidence suggesting the direct involvement of EZH2 in either purine metabolism, RhoGTPase activity, or ribosome biogenesis is available to date.

The current work presents evidence for a previously unrecognized methyl-transferase independent role of EZH2 in melanoma tumorigenesis and invasion. We revealed that cytosolic EZH2 contributes to rRNA metabolism and Rho GTPase activity by regulating cytosolic IMPDH2 tetramerization/ activity and, in turn, promoting GTP in melanoma cells. Sappanone A (SA) inhibits the interaction between EZH2 and IMPDH2 CBS domain, and is anti-clonogenic in melanoma and a range of other cancer types, but not in normal melanocytes and bone marrow progenitor cells.

MATERIALS AND METHODS

Mice

All animal experiments were performed in accordance with the Alfred Research Alliance Animal Ethics Committee protocols #E/1792/2018/M. All mice used in this study were supplied by and housed in AMREP Animal Services. Ei . Eight-week-old female NOD SCID. IL2R-/- Mice (NSG) mice were used for subcutaneous injection of pLV empty vector, shEZH2-3'UTR, shEZH2+EZH2-WT or shEZH2+ EZH2-H689A containing A375 melanoma cells (1x104 cells mixed with 50 ul GFR-Matrigel, n=8 mice per group). Tumours were measured with callipers weekly, and all mice were sacrificed once the first tumour reached 20mm in diameter.

Human melanoma tumor samples

62 human melanoma tumor tissue sections ranging from grade I to IV were obtained from Melanoma Research Victoria (MRV) under the guidelines approved by the

Victorian Government through the Victorian Cancer Agency Translational Research Program.

Cell lines and primary cells

The HEK293, C32, SK-MEL28, IGR39, A375, B16-F10 and IGR37 cell lines were obtained from ATCC and cultured under conditions specified by the manufacturer. C006-M1 cell line was from QIMR Berghofer Medical Research Institute. LM-MEL28, LM-MEL33, LM-MEL43, LM-MEL45 were from Ludwig Institute for Cancer Research [42]. LM-MEL28: B4:F3 is the monoclonal line derived from LM-MEL28 cells in our lab previously. MCF7 and MDA-MB-231 cell lines were provided by Prof Jane Visvader (WEHI), OVCAR3, OVCAR8 cell lines were kindly provided by Prof David Bowtell (Peter MacCallum Cancer Centre), PC3, LNCaP, C4-2 cell lines by A Prof Renea A. Taylor (Monash Biomedicine Discovery Institute), OMM1 was kindly provided by Prof Bruce R. Ksander (Harvard Medical School) and 92.1 cell line by Prof Martine Jager (Leiden University Medical Centre). Mycoplasma tests were routinely performed in our laboratory and short tandem repeat (STR) profiling was conducted by the Australian Genome Research Facility (AGRF) to authenticate the human cell lines.

Chemicals

The chemicals used for treating cells were GSK126 (Selleckchem, S7061), EPZ6438 (Selleckchem, S7128), Sappanone A (Cayman Chemicals, 23205), MPA (Selleckchem, S2487), Ribavirin (Selleckchem, S2504), DZNep (Sigma, S804983) and MS1943 (MedChemExpress, HY-133129); all are listed in Table S1.

Plasmids, Cloning, Overexpression, and siRNA

pCMVHA hEZH2 (#24230) and pLV-EF1a-V5-LIC (#120247) plasmids were purchased from Addgene and MYC/FLAG-hIMPDH2 (#RC202977) plasmid from Origene. EZH2 (1-170), EZH2 (1-340), EZH2 (1-503), EZH2 (1-605) deletion mutants, full length EZH2 (1-751) and IMPDH2 (1-187) deletion mutant were cloned into pLV-EF1a-V5-LIC vector backbone's SrfI/NotI RE using the cloning primers listed in Table S1. pCMVHA hEZH2 and V5-EZH2 vector was used to generate EZH2-H689A mutant vector using the mutagenesis primers listed in Table S1 with QuikChange II site-directed mutagenesis kit (Agilent) following the manufacturer's instructions. Custom designed siRNA oligonucleotides listed in Table S1 were purchased from Bioneer

Pacific. For transient transfection, $25x10^4$ cells were transfected with 2.5 µg of DNA using Lipofectamine 3000 transfection reagent (Invitrogen). For siRNA experiments, $25x10^4$ cells were transfected with 10 nM of the indicated oligonucleotides in Table S1 using the Lipofectamine RNAiMAX transfection reagent (Invitrogen). 72 hours after siRNA transfection, cells were used for functional assays or collected for western blot analysis.

Virus-containing supernatant was collected 48 hours after co-transfection of pCMV-VSV-G, psPAX2, pMD2.G and the EZH2 vectors into HEK293 cells, and then added to the target cells. Stable knockdown and rescue of EZH2 was achieved by lentiviral transduction of EZH2 with V5-EZH2-WT or V5-EZH2-H689A. After transduction, cells were selected for antibiotic resistance with 2 µg/mL puromycin (Sigma Aldrich, #P8833), followed by knockdown using stable short-hairpin interfering RNA (MISSION shRNA, Sigma Aldrich) targeting the 3′UTR of human EZH2 (TRCN0000286227), as previously reported[38].

GST pull-down Assay

GST pull-down assay was performed as previously described[43] with minor modifications. The plasmid GST-EZH2 (1-170), -EZH2 (1-340), -EZH2 (1-503), or –EZH2 (1-605) or GST only was expressed in BL-21 bacteria in the presence of 0.5mM IPTG for 2.5 h at 37ºC. Bacterially expressed GST only (control) or each GST–EZH2 mutant peptide were solubilized in NETN buffer (1% NP-40, 20mM Tris-HCl, pH 8.0, 100mM NaCl, 1mM EDTA) and sonicated in 30 second bursts followed by 30 seconds rest for 15 cycles. Then they were purified by affinity chromatography on Glutathione Magnetic Agarose Beads (Pierce, Thermo Fischer)) and stored in PBS at 4ºC until use. For GST–pull-down assays, purified GST control or GST–EZH2 mutant peptides were mixed with total lysates isolated from HEK293 cells, overexpressing V5-IMPDH2-CBS, grown in serum-fed condition and then incubated for 2 h at 4°C with constant rotation. The lysates from HEK293 cells were used as a source of IMPDH2-CBS domain. After extensive washing of unbound proteins, bound protein was eluted and analyzed by sodium dodecyl–PAGE (SDS–PAGE).

Colmmunoprecipitation and HA/ FLAG pulldown assays

Pellets of $1x10^7$ cells were lysed with 1mL Co-IP Lysis Buffer (300mM NaCl, 50mM Tris HCL pH7.4, 0.5% NP40, 0.1% Sodium deoxycholate, 2% SDS) with PhosSTOP

(Roche) and cOmplete (Roche) rolled at 4°C for one hour. DynaBeads™ Protein G (Thermofisher) were washed three times with Co-IP lysis buffer and chilled in preparation. Lysates were centrifuged at 15,000 RPM for 15 minutes at 4°C and the supernatant was collected, pre-cleared with 20µL of prewashed DynaBeads and incubated on a roller for 1 hour at 4°C. Lysates had pre-cleared beads removed and were split with 500µL for IgG control and 500µL for EZH2 sample, topped to 1 mL with Co-IP lysis Buffer. These were incubated overnight at 4°C with 1:1250 of Rabbit (DAIE) mAB IgG Isotype control or 1:300 of anti-EZH2 (D2C9) XP Rabbit antibody, respectively. After 16 hours of incubation, 35µL of pre-washed DynaBeads were added to IgG control or EZH2 sample and returned to the roller for 2-4 hours incubation at 4°C. Beads were washed with Co-IP buffer once, and then buffers of increasing salt concentrations (Buffer 1, 50mM Tris, pH8.0, 150mM NaCl; Buffer 2, 50mM Tris, pH8.0, 450mM NaCl; and buffer 3, 1M Tris, pH8.0). For Mass Spectrometry, proteins were eluted by resuspending in 150µL of 0.2M Glycine, pH2.5, for 5 minutes on ice and collecting supernatant, which was repeated twice. To the 450 µL of sample, 100 µL of 1M Tris-HCl (pH8.0) was added and the samples were kept at -80°C until LC-MS analysis. For CoIP-WB analysis beads were washed three times with Co-IP Lysis Buffer.

For HA pulldown assays the cells were lysed with 500 µL of IP Lysis Buffer containing cOmplete (Roche) protease inhibitor cocktail and incubated at 4ºC for 35 min on a rotator followed by centrifugation at 15000 rpm for 15 min at 4ºC. 50 µL of the lysates were kept for inputs. 25 µL of Pierce anti-HA magnetic beads (Thermo Fischer Scientific) were added onto the lysate and incubated at RT for 30 minutes on a rotator. Beads were washed with 300 µL of TBST three times and the beads were boiled in 2x SDS-Laemmli Sample Buffer for 10 minutes.

Western blot

Total proteins were extracted from cell lines and tumor xenografts in ice-cold lysis buffer (10mM Tris HCL pH8.0 1mM EDTA 1% TritonX100 0.1% Sodium Deoxycholate 2% SDS 140mM NaCl, protease inhibitors and phosphatase inhibitors). Lysates were prepared after incubation on ice for 1h and centrifugation for 15 minutes cold at 15,000 rpm. Supernatants were boiled in 6x SDS-Laemmli Sample Buffer for 10 minutes. Proteins were run on 4–20% Mini-PROTEAN TGX Stain-Free Protein Gels (BioRad, 4568096) and then transferred to PVDF membrane by wet transfer system.

Membranes were blocked with PBS containing 0.1% Tween-20 and 5% (w/v) skim milk, followed by incubation with the antibodies listed in Table S1. Signals were detected using Clarity ECL Western blotting Substrate (BioRad). Where applicable, signal intensities were quantified by ImageJ densitometry analysis software.

Non-reducing SDS-PAGE

Samples were lysed in 2x Laemmli Sample Buffer without SDS and DTT and run with SDS free running buffer.

DSS Crosslinking

$1x10^6$ cells were precipitated and washed once with 1xPBS. The cell pellet was resuspended in 500 µL of 1xPBS. Cell suspensions were either DMSO control or 1mM DSS (A39267, Thermo Fisher) added and incubated for 30min at RT. Then, the cells were quenched with 50mM Tris-HCl pH:8.0 by incubating for 15min at RT. Finally, the cells were centrifuged, and the cell pellets were boiled in 50 µL of 2x SDS-Laemmli Sample Buffer for 10 min at 95^0C.

Cytoplasmic and nuclear fractionation

Cytoplasmic and nuclear extracts were isolated using a nuclear extraction kit according to the manufacturer's protocol (Affymetrix; Santa Clara, CA) with modifications[43]. Co-IP was performed with anti-EZH2 or anti-IMPDH2 antibody at 4˚C as described in the Co-IP method section. The immune complexes were collected with Protein G-Dynabeads (Thermo Fischer) and washed in lysis buffer. Bound proteins were analyzed by SDS–PAGE and WBs.

RNA isolation and quantitative PCR

Total RNA from cells was extracted using Purelink RNA mini isolation kit according to the manufacturer's instructions (Thermo Fischer Scientific) with the additional Purelink On-Column DNA purification (ThermoFisher Scientific) step. Complementary DNA (cDNA) was synthesized using total RNA (1 µg per reaction) with SuperScript Vilo cDNA synthesis kit (Thermo Fisher Scientific) as per manufacturer's protocol. Quantitative PCR (qPCR) was carried out using Fast SYBR Green Master Mix (Invitrogen) and LightCycler 480 Instrument II (Roche). RNA expression changes were determined using a ΔΔCt method[44]. RPLP0 mRNA was used as an internal control in all qPCR reactions. Table S1 shows the qPCR primers used for IMPDH2, pre-rRNA,

pre-tRNA, pre-GAPDH, p53, CDKN1A, CDKN2A, MDM2, PUMA and RPLP0 mRNA amplifications.

Cell Proliferation, Clonogenicity and Sphere Formation Assay

To measure cell proliferation rates, we plated equal numbers of cells in 6-well plates. Cells were trypsinized and counted on the indicated days by haemocytometer after trypan blue staining.

For clonogenicity assay, cells were fixed with ice-cold absolute methanol for 20 min and air-dried for 15 minutes. Cells were stained with 0.5% Crystal Violet for 20 min at room temperature and then rinsed with tap water to remove excess dye. Five random fields of stained cells were imaged using bright field microscopy at 40 × magnification and average cell numbers per field were plotted as a function of time.

Sphere formation assays were performed as described[43]. Briefly, cells (500 cells per well) suspended in 100 mL ice-cold Matrigel in RPMI medium (1:1 ratio) were overlaid onto the pre-solidified 50% Matrigel in 24-well plates (100 ml per well). Cells were fed with 500 mL RPMI medium containing 10% FBS and grown for 14 days with a change of medium every 3 days. For the SA study, A375 and B16-F10 cells (500 cells/well) were grown on Matrigel and treated either with DMSO (vehicle) or SA in serum-fed conditions for the indicated days. Spheres were imaged and then manually quantified.

Cell senescence β-Gal assay

Cells were fixed and stained with Senescence β-Galactosidase Staining Kit (CST #9860) following the manufacturer's instructions and imaged on a Leica DMIL LED microscope under bright field settings.

3D Matrigel Invasion and Wound Healing Assays

Cells ($1x10^5$ cells per well) were seeded in a 24-well Boyden chamber with an 8-mm filter coated with 20% growth factor reduced Matrigel. Cells were grown in RPMI medium containing 10% FBS for 16, 24 and 48 h at 37°C with 5% CO2. Cells on the inner side of the chamber were gently removed by scraping with a wet cotton swab. Invaded cells at the outer side of the chamber were fixed with 4% formaldehyde for 30 min at RT and rinsed twice with PBS. Cells were stained with 0.5% Crystal Violet for 20 min at RT and then rinsed with tap water to remove excess dye. Analysis was

performed based on the average number of stained cells per field from five random fields at 20x magnification on a Leica DMIL LED microscope.

Wound healing assays were performed by seeding cells in complete media on a 24-well plate for 24–48 h until a confluent monolayer had formed. Linear scratches were made using a sterile 200µl pipette tip. Monolayers were washed three times with PBS to remove detached cells, and then complete media was added. Images of the wound were taken immediately and 24h following wound formation on a Leica DMIL LED microscope under the phase contrast setting. Wound area was measured over time using ImageJ.

RhoA activation assay

RhoA activities were measured in melanoma cells using RhoA G-LISA activation assay kit according to the manufacturer's protocol. Briefly, cells were lysed in ice-cold lysis buffer and quickly cleared by centrifugation. Precision Red Advanced Protein Assay Reagent (Part # GL50) was used to quantify protein contents. Equal amounts of proteins were loaded onto ELISA plates. After several antibody incubation and washing steps the active RhoA bound protein levels were evaluated colorimetrically by OD490 nm absorbance measurement.

Fontana Masson staining

Cells sorted onto slides were fixed with 4% PFA for 20 minutes and washed twice with distilled water for 5 minutes. Then slides were incubated in Fontana silver nitrate working solution (2.5% Silver nitrate, 1% ammonium hydroxide) at 60°C for 2 hours. Slides were rinsed in water three times and incubated with 0.2% gold chloride solution (Sigma-Aldrich) for 2 minutes. Rinsed slides were incubated with 5% sodium thiosulfate for 2 minutes. After rinsing with water twice, slides were counterstained with 10 µg/mL DAPI solution for 5 minutes. Slides were rinsed and mounted with fluorescence mounting medium (Dako).

Schmorl's staining

The samples were dewaxed with 3 x 5-minute histolene washes, and rehydrated in washes of 100%, then 95% and then 75% ethanol for 5 minutes each. Slides were washed with distilled water and placed in Schmorl's Stain for 10 minutes. Slides were washed with water for 1 minute, placed in Eosin in water for 15 seconds, and returned

to constant washing with water for 3 minutes. The slides were finished with 4 x 2-minute washes of 100% ethanol and 3 x 2-minute washes of Histolene. Slides were mounted with DPX Mounting Medium (Thermo Fisher Scientific).

H&E staining was done to evaluate nucleolar sizes[5]. For melanoma patient sample IHC, slides were incubated at 60°C for 1h, dewaxed in histolene, and hydrated through graded alcohols and distilled water. Sections were subjected to antigen retrieval in Antigen Retrieval solution (Dako, pH6 for EZH2, IMPDH2 antibody) at 125° for 3 minutes heated by a pressure cooker. Primary antibody listed in Table S1 was diluted into blocking buffer and slides were incubated overnight at 4°C. After washing with TBST, the slides were incubated with secondary antibody using an ImmPRESS™ HRP Anti-Mouse IgG (Peroxidase) Polymer Detection Kit (Vector Laboratories) for 60 min at RT. Sections were washed with TBST and slides were developed by adding AEC+ High Sensitivity Substrate Chromogen Ready to use (Dako K346111-2).

For immunofluorescence, cells were fixed with 4% PFA diluted in PBS for 15 min at RT, rinsed three times with PBS, and blocked for 1h using blocking buffer (5% normal donkey serum containing 0.3% Triton X-100 in PBS). After blocking, slides were incubated with primary antibody (Table S1) diluted in antibody buffer (5% bovine serum albumin containing 0.3% Triton X100 in PBS) at 4 °C overnight. Slides were washed three times with PBS and incubated with fluorescent secondary antibodies indicated in Table S1. Slides were washed three times with PBS, stained with 10µg/ml DAPI and coverslipped using Fluorescence Mounting Medium (Dako). Slides were imaged using Leica DMIL LED inverted fluorescent microscope or Nikon A1r Plus si confocal microscope.

For proximity ligation assays, cells were seeded on round coverslips. After 24 h of seeding, cells were fixed with 4% PFA for 15 min at RT, rinsed three times with PBS, and blocked for 1 h using blocking buffer(5% normal goat serum containing 0.3% Triton X-100 in PBS). After blocking, slides were incubated with primary antibody diluted in antibody buffer (5% bovine serum albumin containing 0.3% Triton X-100 in PBS) at 4°C overnight. Slides were then washed three times with PBS and incubated with DuoLink PLA probes (Sigma, Cat #DUO92101). The protocol for PLA secondary antibody incubation, ligation, amplification, and washes were performed following the manufacturer's protocol. Slides were imaged using a Nikon A1r Plus si confocal

microscope. Positive signals were normalized to single-primary antibody control (EZH2 or IMPDH2) and image analysis was performed using ImageJ.

PDX Tumor Dissociation

Mice were euthanised with CO2 and tumours were resected. Tumors were manually dissociated in Hank's Balanced Salt Solution (without Ca2+ and Mg2+, HBSS-/-), followed by enzymatic tumour dissociation using the gentleMACS tissue dissociator in Tissue Dissociating media (200 u/mL Collagenase IV, 5 mM $CaCl_2$ in HBSS -/-). Tissue was washed with HBSS-/- and pelleted at 220g for 4 minutes at 4°C, and the supernatant was removed. After this, the pellet was resuspended with 100units/g of DNase and 5mL/g of warmed trypsinEDTA and incubated at 37°C for 2 minutes. Equal volumes of cold staining media were added, and the samples were pelleted at 220g for 4 minutes at 4°C. Supernatant was removed and the pellets were resuspended in cold staining media and filtered with a 40-micron cell strainer. To separate the tumoral cells from mouse stroma, cells were stained with an antibody cocktail of directly conjugated antibodies to mouseCD31 (endothelial cells), mouse CD45 (white blood cells), mouse TER119 (red blood cells) and human HLA-A/B antibodyin staining media on ice for 30 minutes. Labelled cells were resuspended in 2µg/ml DAPI in staining media with 10% FBS and 10uL/mL of DNase. Cells were subsequently analyzed and/or sorted on a FACSFusion (Becton Dickinson).

CD34+ bone marrow progenitor cell isolation and culturing

Donor CD34+ HSPC samples were obtained from normal patients after informed consent in accordance with guidelines approved by The Alfred Health human research ethics committee. Cells from a leukapheresis sample were isolated using Ficoll-Paque PLUS (GE Healthcare) and density centrifugation, followed by NH4Cl lysis to remove red blood cells. A secondary isolation step was completed using CD34 MicroBead Kit (Miltenyi Biotec) performed according to the manufacturer's protocol for positive selection of CD34+ cells from the mononuclear population. Isolated CD34+ cells were cultured in expansion medium (Stemspan SFEM (Stem Cell Technologies 09650), 50ng/ml rhFLt3L (R&D 308-FKN), 50ng/ml rhSCF (R&D 255-SC), 10ng/ml rhIL-3 (R&D 203-IL), 10ng/ml rhIL-6 (R&D 206-IL), 35nM UM171 and 500nM Stemreginin) with or without SA for 4 and 7 days.

Human skin acquisition, single cell suspension, isolation of melanocytes via FACS and melanocyte culture

Epidermal melanocytes were isolated from normal adult human breast skin. The skin samples were provided from Caucasoid donors (age 18 – 72) via The Victorian Cancer Biobank.

Fat was removed from the skin and washed in PBS with Gentamycin (10 µg/mL) and 80% EtOH. Then the skin was cut into small pieces (~5 mm^2) and incubated in Dispase (15 U/mL, Gibco/Thermo Fisher Scientific) with Gentamycin (10 µg/mL) at 4°C overnight. Epidermis was peeled from dermis by forceps and smashed by scissors and incubated in Trypsin/EDTA (0.25%) at 37°C for 10 min to make a single cell suspension of the epidermal cells. After pipetting and addition of fetal bovine serum (FBS) to stop activity of trypsin (final concentration of FBS is 10%), the epidermal single cell suspension was passed through cell-strainers (70 µm then 40 µm). After centrifugation (220g for 5 min) the collected epidermal cells were suspended in the staining medium and viability was validated microscopically with trypan blue.

The collected epidermal cells from skin were incubated with primary antibodies including FITC anti-human CD326 (EpCAM) (1:100, mouse), FITC anti-human CD31 (1:100), FITC anti-human CD45 (1:100), FITC anti-human CD235a (1:100) and PE anti-human CD117 (c-kit) (1:100) in the staining media for 30 min at 4°C. After a wash and centrifuge the cells were suspended in DAPI (2.5 µg/ml) and subjected to FACS analysis (BD FACSAria™ Fusion flow cytometer, BD).

Debris (by morphology plot: FSC-A/SSC-A), doublets (by doublet plot: FSC-H/FSC-W and SSC-H/SSC-W) and dead cells (DAPI+) were excluded.

Ckit+CD326-CD31-CD45-CD235a- fraction was sorted into 1.5 ml microcentrifuge tubes filled with Medium 254 (1 mL).

The sorted primary human melanocytes were plated on HaCaT-derived ECM-coated culture dish and cultured in Medium 254 supplemented with Human Melanocyte Growth Supplement-2 (HMGS-2, including basic FGF, insulin, transferrin, bovine pituitary extract, endothelin-1, FBS, heparin and hydrocortisone, concentrations are proprietary, PMA-free) at 37°C with 10% O2 and 5% CO_2.

RNA-Seq data analysis

FASTQ files were processed using Laxy (https://zenodo.org/record/3767372) which encompasses the RNAsik pipeline (https://joss.theoj.org/papers/10.21105/joss.00583). Briefly, GRCh38 reference genome was used for STAR alignment [45] and gene expression counts were performed using featureCounts [46]. Gene counts were analysed using Degust (https://zenodo.org/record/3501067) for differential expression analysis. Data processing was performed on NeCTAR Cloud Servers, or MASSIVE High Performance Computing (HPC) cluster.

Differential gene expression analysis was performed using edgeR (v.3.32.1). Quasi-likelihood F-test was performed with glmQLFit and glmQLFTest functions. Gene ontology (GO) enrichment test was performed using PANTHER (v16.0) fisher's exact test corrected by false discovery rate (FDR).

TCGA survival analysis

The clinical data and mRNA expression profiles for skin cutaneous melanoma samples in TCGA PanCancer Atlas database were retrieved from MSKCC Cancer Genomics Data Server (CGDS) (http://www.cbioportal.org) [47]. The "high expression" and "low expression" groups for each gene were defined as above or below the median expression level for the cohort respectively. The overall survival (OS) curves were calculated with the Kaplan-Meier method and the statistical significance were tested with the log-rank test. The calculations were performed using the R package 'survival' 3.1-11 and the survival curves were plotted using the R package 'survminer' 0.4.4.

Sample preparation for GTP/XMP analysis

1 x10^7 A375 cells were washed once with 0.9% NaCl and cell pellets were snap frozen prior LC-MS analysis. 200 µL of extraction solvent (2:6:1 $CHCl_3$: MeOH: H_2O) at 4°C was added to the washed cell pellets after which the samples were briefly vortexed, sonicated in an ice-water bath (10 minutes). Samples were then frozen in liquid nitrogen and thawed three times before mixing on a vibrating mixer at 4°C for 10 minutes after which they were subjected to centrifugation (20,000 x g, 4°C, 10 min) and the supernatant transferred to samples vials for prompt (same day) LC-MS analysis.

LC−MS analysis for metabolomics

Samples were analyzed by hydrophilic interaction liquid chromatography coupled to triple quadrupole mass spectrometry (LC−MS). In brief, the chromatography utilized a ZIC-p(HILIC) column (Merck SeQuant ZIC-pHILIC 5um 150 x 4.6 mm, polymeric) and guard (Merck SeQuant ZIC-pHILIC Guard, 20 x 2.1 mm, PEEK coated guard) with a gradient elution of 20 mM ammonium carbonate (A) and acetonitrile (B) (linear gradient time-%B as follows: 0 min-80%, 15 min-50%, 18 min-5%, 21 min-5%, 24 min-80%, 32 min-80%) on a 1290 Infinity II (Agilent). The flow rate was maintained at 300 µL/min and the column temperature 25°C. Samples were kept at 10°C in the autosampler and 5 µL injected for analysis. The mass spectrometry was performed in multiple reaction monitoring (MRM) mode on an Agilent 6495 Triple Quadrupole. Full details are provided in supplementary material. Peak integration was carried out using MassHunter Qualitative Navigator B.08.00 (Agilent).

LC-MS analysis for proteomics

Immunoprecipitated proteins were reduced with 10 mM TCEP (Thermo Fisher), alkylated with 40 mM iodoacetamide (Sigma Aldrich) and digested with sequencing grade trypsin (Promega). Samples were acidified with 1% formic acid (FA) and purified using OMIX C18 Mini-Bed tips (Agilent) prior to LC-MS/MS analysis.

Using a Dionex UltiMate 3000 RSLCnano system equipped with a Dionex UltiMate 3000 RS autosampler, an Acclaim PepMap RSLC analytical column (75 µm x 50 cm, nanoViper, C18, 2 µm, 100Å; Thermo Scientific) and an Acclaim PepMap 100 trap column (100 µm x 2 cm, nanoViper, C18, 5 µm, 100Å; Thermo Scientific), the tryptic peptides were separated by increasing concentrations of 80% acetonitrile (ACN) / 0.1% formic acid at a flow of 250 nl/min for 128 min and analyzed with a QExactive HF mass spectrometer (ThermoFisher Scientific). The instrument was operated in the data dependent acquisition mode to automatically switch between full scan MS and MS/MS acquisition. Each survey full scan (m/z 375–1575) was acquired in the Orbitrap with 60,000 resolution (at m/z 200) after accumulation of ions to a 3 x 10^6 target value with maximum injection time of 54 ms. Dynamic exclusion was set to 15 seconds. The 12 most intense multiply charged ions ($z \geq 2$) were sequentially isolated and fragmented in the collision cell by higher-energy collisional dissociation (HCD) with a fixed injection time of 54 ms, 30,000 resolution and automatic gain control (AGC) target of 2 x 10^5.

The raw data files were analyzed with the MaxQuant software suite v1.6.5.0 [48] and its implemented Andromeda search engine[49] to obtain protein identifications and their respective label-free quantification (LFQ) values using standard parameters. The proteomics data were further analyzed using either Perseus [50] or LFQ-Analyst [51].

Statistical Analysis

Analysis was performed using GraphPad Prism version 8. All analyses were performed using paired or unpaired Student's t-tests as appropriate to the data type. The statistical parameters are reported in figure legends or text of the results. P values less than 0.05 were considered significant.

RESULTS

EZH2 has methyl-transferase independent functions in melanoma tumorigenicity and metastasis *in vitro* and *in vivo.*

We recently reported that EZH2 abundance, but not its methyltransferase activity, may be the key therapeutic target to lower tumorigenic potential and metastasis of low pigmented melanoma cells[35]. To further investigate the methyltransferase independent function of EZH2 in melanoma, we compared the phenotype (cell growth, clonogenicity, invasion) of melanoma cells subjected to reduced EZH2 protein level by siEZH2 knockown, treatment with the EZH2 degrader DZNep, or treatment with the EZH2-methyltransferase inhibitors GSK126 or EPZ-6438.

Although EZH2 methyltransferase inhibitors, GSK126 (2 μM) and EPZ6438 (2 μM) fully inhibited EZH2 methyltransferase activity as measured by H3K27me3 levels (Fig. 1A, S1A and S1B), they had no effect on cell growth, clonogenicity, migration, invasion, or pigmentation in BRAFV600E mutant cell lines A375 and IGR37, but partial effect on NRASQ61K mutant C006-M1 melanoma cells (Fig. 1A-1F and S1A-S1H). On the contrary, siEZH2-mediated knockdown or EZH2 degradation by DZNep reduced cell growth, clonogenicity, migration and invasion *in vitro* (Figure 1A-D, and S1A-1F) and induced pigmentation as a marker of differentiation in all melanoma cell lines tested (Figure S1G, S1H). Overall, we found that specific inhibition of EZH2 methyltransferase activity did not phenocopy the effects of reduced EZH2 protein level

(e.g., siRNA-mediated knockdown, EZH2 degradation by DZNep treatment) in melanoma cells further verifying a methyl-transferase independent function of EZH2 in melanoma. To further examine the methyltransferase-dependent (MTD) and -independent (MTI) transcriptional program of EZH2 on the genome-wide scale, we performed a global expression analysis of B16-F10 murine melanoma cells treated with scrambled control or siEzh2 knockdown in parallel with B16-F10 cells treated with 2 μM GSK126 or DMSO control. We identified 1370 genes that were significantly increased (FDR< 0.01) upon Ezh2 depletion (Figure 1E, 1F). Importantly, 1226 (89.5%) of these EZH2-repressed genes were not upregulated by GSK126 treatment, supporting their being methyltransferase independent (MTI)-Ezh2 repressed target genes (Figure 1F). Further, gene ontology (GO) analysis showed that MTI-Ezh2 repressed target genes are strongly enriched for melanin and cholesterol biosynthesis pathways (Figure 1G). On the other hand, gene expression analysis revealed 1119 genes (FDR < 0.01) that were downregulated upon Ezh2 depletion (Figure 1E-1H). Interestingly, the expression of 1087 (97.1 %) of these Ezh2-activated genes was not changed upon GSK126 treatment, supporting an MTI mechanism in both Ezh2-mediated gene repression and activation (Figure 1H). Further, gene ontology (GO) analysis showed that MTI-Ezh2 induced target genes are strongly enriched for DNA replication and DNA repair pathways (Figure 1I). Overall, this genome-wide transcriptomic data revealed that EZH2 mediates dual transcription programs (MTD and MTI), but mostly (>89%) MTI in melanoma.

Because siRNA might have off-target effects, we next examined the regulatory mechanism utilizing an EZH2 catalytically dead mutant, H689A. A375 cells were treated with control (sh-control) or EZH2-targeting shRNA to deplete endogenous EZH2, which was then subjected to rescue using wild-type (V5-EZH2-WT) or H689A-mutant EZH2 (V5-EZH2-H689A). For this experiment, the shEZH2 that targets the 3' UTR of the EZH2 region was utilized to prevent it from degrading ectopic EZH2 (Figure 2A and S2A). shEZH2 3′UTR knockdown reduced A375 and IGR37 melanoma cell clonogenicity, invasion and wound healing capacity that was rescued by the ectopic expression of V5-EZH2-WT and V5-EZH2-H689A to similar extent (Figure 2B-D and S2B-C). Moreover, pigmentation was induced by EZH2 knockdown, and this was reversed by ectopic expression of V5-EZH2-WT and V5-EZH2-H689A (Figure S2B). As expected based on our *in vitro* results, A375 expressing shRNA against EZH2

formed smaller tumors than controls when implanted into NSG mice (Figure 2E, F and S2D). Validating the dispensable role for EZH2 methyltransferase activity on cell proliferation observed *in vitro*, primary tumors formed by V5-EZH2-WT and catalytically dead V5-EZH2-H689A overexpression were of similar size (Figure 2E, F and S2D). In a complementary approach, we tried to identify the EZH2 domain that can rescue the shEZH2 knockdown phenotype by overexpression of EZH2 deletion mutants (Figure 2G). We showed that shEZH2 3′UTR knockdown reduced A375 melanoma cell clonogenicity was rescued partially and invasion was rescued fully by overexpression with N-terminal domain of EZH2 (1-340) [clone 2] that lacks the SET domain enzymatic site (Figure 2H-J). Altogether, these data document that a MTI function of N-terminal domain of EZH2 is critical for the tumorigenicity and invasion in melanoma.

N-terminal domain of cytosolic EZH2 interacts with IMPDH2 through the IMPDH2-CBS domain in a PRC2- and methylation-independent manner.

To characterize the MTI actions of EZH2 in melanoma, we examined EZH2 interacting partners in melanoma cells by EZH2-CoIP coupled with LC-MS. As expected, PRC2 complex proteins were identified as EZH2 binding partners (Figure 3A and Table S2) together with the ubiquitin degradation pathway proteins UBR4 and NPLOC4, Kinesin 1 complex proteins including KIF5B, KLC1, KLC2 and KLC4, and Inosine-5'-monophosphate dehydrogenase 2 (IMPDH2), all being within the top ten most abundant binding partners in all five human melanoma cells lines tested (four *BRAF*^{V600E} mutated and one *NRAS*^{Q61K} mutated) and one *BRAF*^{V600E} PDX tumor (Figure 3A and Table S2). In this study, we focused on the role of the IMPDH2-EZH2 interaction in melanoma progression and metastasis, because the role of IMPDH2 in melanoma has not yet been studied in detail. Firstly, we found that IMPDH2 protein level is upregulated in human melanoma cells compared to normal human melanocytes (NHM) (Figure S3A) and high IMPDH2 expression is correlated with poor melanoma survival (p= 0.01, cbioportal) (Figure S3B). Then, we validated and investigated the mechanistic details of the interaction between EZH2 and IMPDH2 using multiple independent and complementary strategies. First, we verified endogenous EZH2-IMPDH2 interaction in A375 cells and PDX tumors by reciprocal Co-IP experiments (Figure 3B and S3C). This interaction was reproducibly seen in EZH2 enzyme-inhibited conditions after 3 days GSK126 or EPZ6438 treatment,

showing that EZH2 interacts with IMPDH2 independent of its methyltransferase activity (Figure 3SD). Exogenously expressed EZH2 (HA-EZH2) interacts with both full length IMPDH2 (MYC/FLAG-IMPDH2) protein in HEK293 cells (Figure 3SE) and the CBS domain of IMPDH2 [V5-IMPDH2-(1-187)] in A375 cells (Figure 3C). GST pull down assays showed that the CBS domain of IMPDH2 interacts with the N-terminal EED binding domain (1-170) of EZH2 (Figure 3D, 3E). Next, we verified that this N-terminal portion (1-170) of EZH2 is responsible for the interaction with full length IMPDH2 using exogenously expressed V5-EZH2 deletion mutants together with MYC/FLAG-IMPDH2 (Figure 3F). Ligation proximity assays (LPA) with confocal imaging showed that 60% of the cells showed cytosolic EZH2-IMPDH2 interaction with the average of 15 foci per cell (< 40nm apart) and 40% of the cells showed both cytosolic and nuclear interaction with the average of 4 foci per cell in melanoma cells (Figure 3G). These results were further verified by western blotting of separated cytosolic and nuclear protein fractions (Figure 3H) and multiplex immunofluorescence in multiple melanoma cells (Figure 3SF). Although our data demonstrated that EZH2 binds to all PRC2 complex elements (SUZ12, EED, JARID2, AEBP2) by LC-MS and to SUZ12 by LPA studies, we found that IMPDH2 does not interact with SUZ12 in the cytosol, whereas 10% of the cells show PLA positive loci in the nucleus with the average of 4 foci per cell (Figure 3G). Furthermore, we were unable to detect IMPDH2 methylation in EZH2 Co-IPs by mass spectrometry (Table S3). Together, these data clearly indicated that although EZH2 is mostly localized in nuclei, its N-terminal domain interacts directly with IMPDH2 via the IMPDH2-CBS domain, predominantly in the cytosol, and independently of PRC2 complex formation or methylation function in melanoma cells.

Cytosolic EZH2 is sufficient for melanoma invasion *in vitro* and tumorigenesis *in vivo*.

To test the relevance of cytoplasmic EZH2 to melanoma tumorigenicity and metastasis we developed an EZH2 mutant lacking the nuclear localization domain (EZH2-ΔNLS). To avoid the contribution of endogenous EZH2 we first generated A375 cells with stable 3′UTR EZH2 knockdown followed by rescue with full length (V5-EZH2-WT) and V5-EZH2-WT-ΔNLS mutant lentiviral constructs. V5-EZH2-WT-ΔNLS expression was mostly cytoplasmic and abolished nuclear EZH2 methyltransferase activity on histone H3K27 (Figure S3G). A375 shEZH2 melanoma cells and xenograft

tumors displayed reduced invasion and tumorigenicity but this was restored by V5-EZH2-WT-ΔNLS to levels similar to that of WT-EZH2 (Figure 3I, 3J and S3H). Moreover, overexpression of cytosolic EZH2 lacking methyltransferase activity (V5-EZH2-H689A-ΔNLS) also restored the invasive phenotype in shEZH2 A375 cells to levels comparable to those achieved with V5-EZH2-WT-ΔNLS. Collectively, these data reveal that cytoplasmic EZH2 expression is sufficient to promote melanoma cell invasion and tumorigenicity irrespective of EZH2 methyltransferase function.

p38-dependent phosphorylation of EZH2 at T367 residue has been shown to induce cytosolic localization of EZH2 in breast cancer cells[38]. Although the PTM analysis of EZH2 mainly showed CDK1/2 and GSK3β-dependent phosphorylation sites, two sites acted upon by unknown kinases and a small percentage of p38 phosphorylation sites, none of them showed a significant difference in their phosphorylation percentages between cytosolic and nuclear EZH2 (Figure S3I, Table S4).

Cytosolic EZH2 moves IMPDH2 to the cytoplasm and increases its tetramerization and total protein level methyltransferase independently.

Next, we investigated the effect of EZH2-IMPDH2 interaction on the IMPDH2 protein level, localization, and its tetramerization/activity. Stable EZH2 knockdown slightly decreased total IMPDH2 protein level, but not mRNA expression, that was later rescued by the overexpression of EZH2 (1-340) [clone 2] (Figure S3J). Fractionation and Co-IF experiments showed that stable or transient EZH2 knockdown moved both endogenous IMPDH2 and exogenously expressed IMPDH2-CBS domain to nuclei in A375 cells (Figure 3K, S3K, S3L). Conversely, overexpression of cytosolic wild-type EZH2 (V5-EZH2-WT-ΔNLS) or cytosolic EZH2 (1-340) [clone 2], preferentially shifts IMPDH2 into the cytosol when compared to overexpression of wild type EZH2 (V5-EZH2-WT) in endogenous EZH2 silenced A375 cells (Figure 3L, S3M). This effect is independent of its methyltransferase activity as similar effects on IMPDH2 localization were observed comparing V5-EZH2-H689A to V5-EZH2-WT or comparing V5-EZH2-H689A-ΔNLS to V5-EZH2-WT-ΔNLS (Figure 3L and S3G).

Because tetramerization is an essential step in functional activation of IMPDH2 protein [13,16,52], we investigated the effect of EZH2 on IMPDH2 tetramerization in A375 cells. Cross-linked A375 whole-cell extracts showed that IMPDH2, but not IMPDH1

tetramers were decreased by stable/ transient EZH2 knockdown which was rescued by both overexpression with wild-type and methyltransferase deficient EZH2 full length and EZH2 (1-340) [clone 2] (Figure 3M, S3N and S3O). In summary, these data showed that cytosolic EZH2 retains IMPDH2 in the cytosol and increases its tetramerization and total protein level via a mechanism unrelated to methyltransferase activity.

IMPDH2 induces clonogenecity/invasion in melanoma cells by regulating ribosome biogenesis and actomyosin contractility via cellular GTP level regulation.

Next, we assessed the impact of pharmacological and genetic inhibition of IMPDH2 on melanoma cell clonogenicity and invasion. Treatment with mycophenolic acid (MPA) or ribavirin, a pan-IMPDH inhibitor[12,53,54], dramatically decreased cell proliferation, clonogenicity in 3D-matrigel and invasion that was rescued by guanosine addition in all the tested melanoma cells regardless of B-Raf or N-Ras mutational status, demonstrating a GTP dependent pro-proliferative and pro-invasive role of IMPDH in melanoma cells (Figure 4A-E and 4A-S4E). MPA and ribavirin also induced hyper-pigmentation/differentiation and senescence shown by β-gal staining (Figure S4F, S4G). Next, we used siRNA silencing of IMPDH2 to evaluate its specific contribution to melanoma cell proliferation and invasion *in vitro*. In parallel with the inhibitor data, IMPDH2 silencing retarded melanoma cell proliferation and invasion that was restored by guanosine addition (Figure 4F, 4G, S4H and S4I). Taken together, these results reveal the essential role of IMPDH2 activity in the proliferation and invasiveness of melanoma cells via GTP synthesis *in vitro*.

IMPDH2-dependent GTP biosynthesis has been shown to support primarily rRNA and tRNA synthesis in GBM[7]. Many tumor cells increase Pol I activity[7,55-57] and GTP-dependent Pol I activation has been shown in several tumor types[58,59]. We examined RNA synthesis rates by qRT-PCR and found that both MPA treatment and IMPDH2 silencing blunted pre-rRNA (Pol I transcript), and pre-tRNAI13 (Pol III transcript), but not pre-GAPDH mRNA (Pol II transcript) expression levels in A375 cells in a time dependent manner (Figure 4G and S4I). Then, we focused on rRNA synthesis (ribosome biogenesis) and showed that MPA treatment and IMPDH2 silencing triggered the nucleolar stress response characterized by delocalization of nucleolin

and induction of the p53 pathway in A375, B16-F10, C006-M1 and B4:F3 cells (Figure 4H, 4I, S4J, S4K and S4L), with both effects reversed by guanosine addition (Figure 4H, 4I). We conclude that IMPDH2 regulates ribosome biogenesis in melanoma cells via *de novo* GTP synthesis.

GTP is also essential for G-protein activity [11]. Next, we focused on Rho-GTPases that regulate formation and contractility of the actomyosin cytoskeleton via ROCK I/IIactivation and phosphorylation of MLC2 in myosin II, thereby influencing migration, metastatic colonization and amoeboid invasion in melanoma [3,4,60]. MPA treatment and IMPDH2 silencing reduced RhoA activity and phospho-MLC2/F-actin levels (Figure 4J and S4M). Guanosine restored them back to control levels (Figure 4J and S4M) suggesting that IMPDH2 regulates actomyosin contractility by *de novo* GTP synthesis in melanoma.

EZH2 regulates cellular GTP levels via IMPDH2 and guanosine rescues siEZH2-reduced clonogenicity/invasion phenotype by regulating rRNA metabolism and Rho GTPase activity

IMPDH2 is the rate-limiting enzyme in the production of GTP[61-63]. Because we have shown that EZH2 regulates IMPDH2 tetramerization/activity, we checked the contribution of EZH2 on cellular GTP levels in melanoma. Stable EZH2 knockdown reduced GTP levels by 50% in A375 cells and the GTP level turned to basal level upon overexpression with N-terminal domain of EZH2 (1-340) [clone 2] that was previously shown to be the docking site for IMPDH2 (Figure 5A). In addition, stable EZH2 knockdown reduced cell proliferation, migration and invasion but these effects were reversed by guanosine addition (Figure 5B and S5A-D). Moreover, EZH2-WT or -H689A overexpression induced cell proliferation and invasion which was reduced to shEZH2 levels after IMPDH2 silencing; again, these effects were rescued by guanosine addition, clearly showing that EZH2 contributes to cell proliferation and invasion through IMPDH2-induced GTP synthesis (Figure 5C, 5D and S5C-D).

Cellular GTP levels are critical for diverse functions in cancer cells, including rRNA metabolism and GTPase activities. EZH2 knockdown downregulated rRNA synthesis and ribosome biogenesis that resulted in p53 induction in melanoma cells (Figure 5E, S5E and S5F). EZH2 induced ribosome biogenesis was reversed by guanosine addition (Figure S5E). Having demonstrated the importance of IMPDH2-

derived GTP in actomyosin contractility, we next examined the effect of stable EZH2 knockdown on actomyosin contractility. RhoA activity and phospho-MLC2 levels were lowered by EZH2 silencing (Figure 5F, 5G, S5G, S5H and S5I) but phospho-MLC2 levels were restored by guanosine addition (Figure 5H and S5G). Like stable EZH2 knockdown, transient EZH2 silencing by two siEZH2 constructs and EZH2 degradation by DZNep and MS1943 reduced phospho-MLC2 levels, but this effect was not observed by the EZH2 specific methyltransferase inhibitors, GSK126 and EPZ-6438 (Figure S5J, S5K) verifying the methyltransferase independent role of EZH2 on RhoA dependent myosin II activation.

In summary, EZH2 regulates cellular GTP levels via IMPDH2 and guanosine rescues shEZH2-reduced clonogenicity/migration/invasion by upregulating rRNA metabolism and RhoA dependent myosin II activation.

The percentage of cytosolic EZH2/IMPDH2^{+} cells and nucleolar size are higher in stage 4 metastatic melanoma patients.

The nucleolar size in shEZH2-3'UTR A375 tumor specimens was significantly decreased compared to wild-type A375 tumors. The nucleolar size was reversed by overexpression with wild-type or methyltransferase-deficient forms of EZH2 *in vivo* (Figure S5L). In the Protein Atlas database (https://www.proteinatlas.org/ENSG00000178035-IMPDH2/tissue/skin#img) IMPDH2 is expressed in the nuclei of normal human melanocytes where EZH2 staining is undetectable. We verified this data using isolated normal human melanocytes and melanoma samples showing that IMPDH2 expression is either not detectable or nuclear in the small percentage of normal melanocytes and stage I melanoma samples in which EZH2 is not expressed (Figure 5I and S5M). In stage IV metastatic melanomas, however, cytosolic EZH2 and IMPDH2 expressions were significantly increased and correlated with nucleolar size, which is an indicator for ribosome biogenesis (Figure 5I). Together, these data suggest that the cytosolic EZH2/IMPDH2 complex directly contributes to ribosome biogenesis in metastatic melanoma cells and metastatic human melanoma specimens.

Sappanone A (SA) reduces EZH2/IMPDH2 interaction, IMPDH2 tetramerization and nuclear translocation of IMPDH2.

As we showed that EZH2 interacts with CBS domain of IMPDH2 (Figure 3C), we searched the literature for drugs that can inhibit this interaction. A natural small-molecule, called Sappanone A (SA) has been demonstrated to specifically inhibit IMPDH2 by directly targeting the conserved cysteine residue 140 (Cys140) in the CBS domain of IMPDH2. SA induces an allosteric effect on the catalytic pocket and suppresses IMPDH2 activity. We examined the effect of SA on EZH2/IMPDH2 interaction and the related melanoma phenotype. SA inhibited both endogenous EZH2/IMPDH2 interaction and exogenous EZH2/IMPDH2-CBS domain interaction and IMPDH2 tetramerization in A375 and B16-F10 cells in a dose-dependent manner (Figure 6A-C and S6A-B). In addition, 10 to 20 μM of SA also induced IMPDH2 nuclear localization significantly in A375 cells (Figure 6D and S6C). These data suggest that EZH2/IMPDH2 interaction can be targeted by SA.

Pharmacological inhibition of EZH2/IMPDH2 interaction by SA attenuates the growth and invasion abilities of melanoma cells *in vitro*.

Next, we tested the effect of SA on melanoma cell growth and invasion in 2D culture and 3D matrigel. SA reduced melanoma cell proliferation and clonogenicity dose-dependently that was reversed by guanosine addition in both A375 and B16-F10 cells (Figure 6E and S6D, S6E). The induction of cell proliferation and invasion by EZH2-WT overexpression in the shEZH2 background were reduced to that of shEZH2 level after 5 μM SA treatment and were later rescued by guanosine addition clearly showing that EZH2 contributes to cell proliferation and invasion through IMPDH2-induced GTP synthesis (Figure 6F and S6F). In these cells, 5 μM and 10 μM SA reduced 3D matrigel spheroid numbers and sizes by preventive therapy (SA treatment was started 16h post seeding) (Figure 6G-I and S6F-H). SA-induced growth inhibition was irrreversible, because after 7 days of drug washout, only one resistant colony emerged in B16-F10 cells, but none in A375 cells (Figure 6G, 6H). Moreover, SA significantly reduced A375 and B16-F10 spheroid sizes and invasive spheroid numbers in 3D matrigel using therapeutic approach in which cells were treated with the drug 6 days post-seeding (Figure 6J-L and S6J-S6K). SA also induced ribosomal stress and reduced myosin II activation shown by anti-NCL and anti-p-MLC2 staining, respectively, in A375 cells (Figure 6M and S6L). Based on LC/MS data IMPDH2 was detected in EZH2 Co-IP complex isolated from $CD34^+$ bone marrow progenitor cells, although we could not verify this interaction by CoIP coupled WB using the same

stringency conditions as in other cancer cells pointing out the weaker interaction in blood progenitor cells (Table S2 and Figure 6N). In parallel, SA treatment has no cytotoxic effect on the blood progenitor cells in a time-dependent manner (Figure 6O). In addition, SA treatment of human melanocytes for 7 days at 2 to 5 μM did not show significant cell growth attenuation (Figure 6P). These data suggest that pharmacological inhibition of EZH2/IMPDH2 interaction by SA attenuates the growth and invasion abilities of melanoma cells by regulating rRNA metabolism and actomyosin contractility without melanocyte and blood cell toxicity.

EZH2-IMPDH2 interaction is commonly seen in uveal melanoma, breast, prostate, ovarian cancer, and SA attenuates their growth in *vitro*.

High EZH2 and IMPDH2 protein levels have been linked to almost all the solid cancers [10], although their interaction has not been shown in the literature yet. First, we examined EZH2 and IMPDH2 protein levels and their interactions in uveal melanoma (UM: 92.1 and OMM1), ovarian cancer (OCa: OVCAR-3 and OVCAR-8), breast cancer (BCa: MCF7 and MDA-MB-231), and prostate cancer (PCa: LNCaP and C4:2) cell lines. EZH2/IMPDH2 interactions were commonly seen in all cancer cell lines tested (Figure 7A-D and S7A-D). In addition, cytosolic EZH2 interacts with cytosolic IMPDH2 in all cell lines tested (Figure 7E and S7E). Next, we tested the inhibitory effect of SA on EZH2/IMPDH2 interactions and IMPDH2 activity in OMM1 (UM), OVCAR-8 (OCa), MDA-MB-231 (BCa), PC3 (PCa) cell lines. Like melanoma cells, SA reduced EZH2/IMPDH2 interactions (Figure 7F, 7G, S7F and S7G) and IMPDH2 tetramerizations in uveal melanoma, ovarian cancer, breast cancer and prostate cancer cells (Figure S7H-K). Both EZH2 degradation by MS1943 and EZH2/IMPDH2 dissociation by SA inhibits cell growth in cancer cell lines, OMM1, OVCAR-8, MDA-MB-231, C4-2 at the IC50 values below 5 μM, whereas EZH2 inhibition by GSK126 has no discernible impact on cell growth up to 10 μM doses (Figure 7H-K). These data suggest that in addition to cutaneous melanoma, EZH2 has methyltransferase independent function/s in uveal melanoma, breast, ovarian and prostate cancer and cytosolic EZH2/IMPDH2 interaction is a novel druggable target in these cancers.

Collectively, these data support a model in which nuclear EZH2 mediates transcriptional silencing and concomitantly, cytosolic EZH2 contributes to the activation of IMPDH2 mediated GTP synthesis that facilitates ribosome biogenesis and actomyosin contractility contributing to melanoma progression and metastasis (Figure 7L). We propose that the molecular mechanism through which EZH2 activates

IMPDH2 mediated GTP synthesis is methyltransferase independent and involves IMPDH2 cytosolic sequestration and tetramerization.

DISCUSSION

EZH2 is a bona-fide oncogene in cutaneous/ uveal melanoma[24-28,64], breast[65], prostate[66], and ovarian cancer[67], responsible for imparting proliferation, migration, and invasion abilities, but the mechanisms are incompletely understood. Previous melanoma literature showed that EZH2 controls melanoma growth and metastasis through silencing of distinct tumour suppressors, such as ciliary genes and AMD1 in N-Ras mutant tumors[27,28] and it also controls mechanisms of adaptive resistance to immunotherapy[30]. Recently, it has been shown that combination of EZH2 plus MEK inhibitors markedly reduces tumor burden in NRAS mutant cells, but not BRAF mutant cells[68] pointing out the possible methyl-transferase independent function/s of EZH2 in BRAF mutant melanomas that is consistent with our findings in which NRAS mutant melanoma cell line shows partial inhibition of metastasis and clonogenicity upon EZH2 inhibition. In contrast, BRAF mutant melanoma cells are resistant to the EZH2 enzymatic inhibitors, but sensitive to EZH2 silencing. We can speculate that methyltransferase dependent functions of EZH2 may dominate its non-enzymatic function in NRAS mutant tumors due to the lower expression levels of IMPDH2 and EZH2 in NRAS mutant cell lines than that of BRAF mutant cell lines.

Recently, uveal melanoma cells have been shown to be resistant to EZH2 inhibition[69] unless the inhibitors was used supraphysiological doses[70]. Triple-negative breast cancer cell line, MDA-MB-231 cells and castration-resistant prostate cancer cell lines, C4-2 and DU145 have been also stated to be resistant to EZH2 inhibition, but sensitive to EZH2 silencing which have been reported to be driven by non-enzymatic functions for EZH2 [38,66,71]. Overall, our data that is consistent with these literature findings revealed a novel non-enzymatic function of EZH2 in these solid cancers. Through an unbiased proteomics approach, in this study we uncovered methyltransferase-independent binding partners of EZH2 in multiple melanoma cells. Among the top EZH2-binding interactors is IMPDH2, the critical enzyme in *de novo* GTP synthesis. In this study, we also showed that EZH2/IMPDH2 interaction is commonly seen in uveal melanoma, breast, prostate, and ovarian cancer cells revealing a novel non-enzymatic, but GTP-dependent function of EZH2 via IMPDH2

interaction in other solid cancers. Our findings may shed light into a common mechanism of EZH2 in human cancer.

Cytoplasmic EZH2 has been observed previously in murine fibroblasts where it retains methyl-transferase activity and regulates actin polymerization[36]. In leukocytes, EZH2 was shown to methylate the cytoplasmic protein talin-1 to enhance migration by inhibiting the binding of talin-1 to F-actin[72]. p38-dependent phosphorylation of EZH2 at T367 residue has been shown to induce cytosolic localization of EZH2 in breast cancer cells to interact with cytoskeletal proteins that promotes metastasis[38]. Likewise, cytoplasmic EZH2 expression has been observed in prostate cancer cells[37]. Prior to our study, the existence of the cytosolic EZH2 and its role in the metastatic ability of melanoma cells were unknown. Our PLA assay, cytosolic/nuclear fractionation experiments and IHC of human melanoma samples clearly showed cytosolic localization of EZH2 in multiple metastatic melanoma cells. In our LC/MS study, PTM analysis of EZH2 proteins isolated from cytosolic and nuclear compartments did not show significant phosphorylation differences. Despite of the evidence that EZH2 is localized in the cytoplasm of melanoma cells, the mechanism of cytosolic EZH2 shuttling has remained unexplored in this study.

Nuclear Drosophila IMPDH has been shown to be accumulated during the G2 phase of the cell cycle or following replicative/ oxidative stress and to be bound to single-stranded, CT-rich DNA sequences via its CBS domain[73-77]. Thus, in the nuclei, IMPDH acts as the transcriptional regulator of the expression of histones and E2F genes in which its enzymatic activity is dispensable[77]. Interestingly, SA that binds to CBS domain of IMPDH2 was discovered to reduce pigmentation via repressing tyrosinase gene expression in mouse melanoma cells[78]. In this study, we observed small percentage of melanoma cells with nuclear IMPDH2 that can interact with SUZ12 and nuclear localization of IMPDH2 upon EZH2 knockdown was enhanced significantly. Meanwhile, siEzh2 RNAseq data shows that pigmentation-related gene expressions (*Tyr, Oca2, Trp1*) were upregulated methyltransferase independently. Our unpublished observation also revealed that *tyrosinase* gene promoter bound IMPDH2 level was enhanced upon EZH2 knockdown. All these evidences conferred that EZH2 may regulate pigmentation-related gene expressions via regulating IMPDH2 nuclear localization. We cannot exclude the possibility that EZH2 manipulation may induce oxidative stress that eventually induces nuclear IMPDH2 localization in melanoma cells. In normal melanocytes where EZH2 is not expressed;

we observed nuclear IMPDH2. Our hypothesis is that in the absence of EZH2 nuclear IMPDH2 may act as an activator of melanocyte differentiation/ pigmentation-related genes in normal melanocytes. During melanoma progression, augmented cytosolic EZH2 protein facilitates IMPDH2 accumulation in the cytosol and increased its activity/protein level. In summary, cytosolic EZH2 may switch differentiation-inducing nuclear IMPDH2 into proliferation-inducing cytosolic IMPDH2.

Increased rRNA synthesis[79] and nucleolar hypertrophy[6] have both long been recognized as features of malignant transformation. Ribosome biogenesis/ rRNA synthesis has been shown to be one of the most enriched pathways in IMPDH2 correlated gene enrichment analysis in TCGA cutaneous melanoma dataset (data not shown). Our data revealed that the activation of IMPDH2 by EZH2 interaction induced de novo GTP synthesis that enhances rRNA synthesis and stimulates nucleolar hypertrophy in metastatic melanoma cells.

Kauffmann et al.,[80] identified a gene-profile signature for human primary malignant melanoma associated with metastasis to distant sites and poor prognosis. Among the most significant pathways associated with progression to metastasis are the DNA replication and the DNA repair pathways[80]. In our study, we identified DNA replication and DNA repair pathways are regulated transcriptionally by EZH2 methyltransferase independently in melanoma. The detail of this mechanism needs to be investigated.

Although trials of pan-IMPDH inhibitors, such as MPA, tiazofurin and benzamide riboside, have been conducted in patients with leukemia and multiple myeloma with very promising results[81-84], studies were terminated due to neurotoxic side effects[85-87], because IMPDH2 is mainly expressed in rapidly proliferating immunocytes, rather than the “housekeeping” type I isoform IMPDH1 in normal human leukocytes and lymphocytes[88,89]. MPA has been shown recently to have more hematological side effects than IMPDH2 specific inhibitor, SA in vivo[16]. Although we displayed that MPA is anti-tumorigenic and anti-metastatic in melanoma cells, SA can be a better treatment option against melanoma in clinical trials with fewer side effects because we demonstrated low or no EZH2/IMPDH2 interaction in $CD34^+$ human blood progenitor cells compared to melanoma cells by LC-MS and coimmunoprecipitation (Table S2) and SA treatment has no anti-proliferative effect on these cells highlighting the significance of SA in clinical trials to eliminate hematological side effects. To our

knowledge, this is the first example of the selective IMPDH2 inhibitor usage for melanoma treatment.

Previous reports show that cMyc and MITF increases IMPDH1 and IMPDH2 expression levels[18,90-92]. However, cMyc/ MITF itself may not explain the rather selective upregulation of IMPDH2 in cancer cells; therefore, it has been suggested that additional regulatory mechanisms of IMPDH2 upregulation is not avoidable. In this study, we identified a novel posttranslational regulatory mechanism of IMPDH2 activity via EZH2 interaction not only in melanoma but also in several solid cancers.

RhoA/ROCK/myosin II pathway is a key regulator of invasive and metastatic behavior of melanoma cells [3,4,60,93]. In this study, we identified EZH2 as the main regulator of RhoAGTPase activity and actomyosin contractility via RhoA/ROCK/myosin II activation. EZH2 exerted this function via GTP synthesis by IMPDH2 activity/localization modulation in melanoma. However, we have not checked the same modulatory effect of EZH2 in other solid cancers.

In conclusion, EZH2 contributes to rRNA metabolism and actomyosin contractility by cytoplasmic complex formation with IMPDH2 to promote GTP in melanoma cells. Thus, this novel non-enzymatic, but GTP-dependent function of EZH2 induces tumorigenesis and metastasis in melanoma cells. Further detailed studies on understanding EZH2/IMPDH2 interaction interface may open new avenues for developing effective therapy for melanoma and other types of cancers where this interaction was commonly seen.

Author Contributions

G.K-A. and M.S. conceived and designed the experiments. G.K-A., F.N., P.S., Y.Z., C.H., C.B., I.L., J.G.C., G.P. and C.C. performed the experiments. P.Z. and N.C.W. analyzed the bioinformatics data. R.B.S and C.H. analyzed the proteomics data. S.M.M analyzed the melanoma patient IHCs. M. Andrews and M. Ameratunga helped for the editions of the manuscript. A.W. provided bone morrow cells. G.K-A. wrote the paper. M.S. conceived, initiated, and supervised the project.

Acknowledgements

The authors would like to thank Scott Coutts from the Monash University Micromon Genomics facility for the RNAseq experiment, the members of the Monash eResearch Centre (MeRC) for access to MASSIVE High performance computing

cluster and data storage and AARNet NeCTAR Research Cloud for compute processing capability. We thank Prof David Bowtell for ovarian cancer cell lines, A Prof Renea A. Taylor for prostate cancer cell lines, Prof Bruce R. Ksander for OMM1 cells, Prof Martine Jager for 92.1 cancer cells and Magdaline Costa, Geza Paukovics, Eva Orlowski-Oliver for helping us the FACS experiments that were carried out in the AMREPFlow core flow cytometry facility. We thank the Melanoma Research Victoria through the Victorian Cancer Agency Translational Research Program for providing us melanoma patient sample blocks.

REFERENCES

1. Dang, C.V. Links between metabolism and cancer. *Genes Dev* **26**, 877-890 (2012).
2. Wawrzyniak, J.A.*, et al.* A purine nucleotide biosynthesis enzyme guanosine monophosphate reductase is a suppressor of melanoma invasion. *Cell Rep* **5**, 493-507 (2013).
3. Sanz-Moreno, V.*, et al.* Rac activation and inactivation control plasticity of tumor cell movement. *Cell* **135**, 510-523 (2008).
4. Sanz-Moreno, V.*, et al.* ROCK and JAK1 signaling cooperate to control actomyosin contractility in tumor cells and stroma. *Cancer Cell* **20**, 229-245 (2011).
5. Ruggero, D. & Pandolfi, P.P. Does the ribosome translate cancer? *Nat Rev Cancer* **3**, 179-192 (2003).
6. Ruggero, D. Revisiting the nucleolus: from marker to dynamic integrator of cancer signaling. *Sci Signal* **5**, pe38 (2012).
7. Kofuji, S.*, et al.* IMP dehydrogenase-2 drives aberrant nucleolar activity and promotes tumorigenesis in glioblastoma. *Nat Cell Biol* **21**, 1003-1014 (2019).
8. Donizy, P., Biecek, P., Halon, A., Maciejczyk, A. & Matkowski, R. Nucleoli cytomorphology in cutaneous melanoma cells - a new prognostic approach to an old concept. *Diagn Pathol* **12**, 88 (2017).
9. Drygin, D.*, et al.* Targeting RNA polymerase I with an oral small molecule CX-5461 inhibits ribosomal RNA synthesis and solid tumor growth. *Cancer Res* **71**, 1418-1430 (2011).
10. Kofuji, S. & Sasaki, A.T. GTP metabolic reprogramming by IMPDH2: unlocking cancer cells' fuelling mechanism. *J Biochem* **168**, 319-328 (2020).
11. Wennerberg, K., Rossman, K.L. & Der, C.J. The Ras superfamily at a glance. *J Cell Sci* **118**, 843-846 (2005).
12. Hedstrom, L. IMP dehydrogenase: structure, mechanism, and inhibition. *Chem Rev* **109**, 2903-2928 (2009).
13. Zhang, R.*, et al.* Characteristics and crystal structure of bacterial inosine-5'-monophosphate dehydrogenase. *Biochemistry* **38**, 4691-4700 (1999).
14. Johnson, M.C. & Kollman, J.M. Cryo-EM structures demonstrate human IMPDH2 filament assembly tunes allosteric regulation. *Elife* **9**(2020).
15. Sintchak, M.D.*, et al.* Structure and mechanism of inosine monophosphate dehydrogenase in complex with the immunosuppressant mycophenolic acid. *Cell* **85**, 921-930 (1996).
16. Liao, L.X.*, et al.* Highly selective inhibition of IMPDH2 provides the basis of antineuroinflammation therapy. *Proc Natl Acad Sci U S A* **114**, E5986-E5994 (2017).
17. Caputo, E.*, et al.* Characterization of human melanoma cell lines and melanocytes by proteome analysis. *Cell Cycle* **10**, 2924-2936 (2011).

18. Mannava, S.*, et al.* Direct role of nucleotide metabolism in C-MYC-dependent proliferation of melanoma cells. *Cell Cycle* **7**, 2392-2400 (2008).
19. Kiguchi, K., Collart, F.R., Henning-Chubb, C. & Huberman, E. Induction of cell differentiation in melanoma cells by inhibitors of IMP dehydrogenase: altered patterns of IMP dehydrogenase expression and activity. *Cell Growth Differ* **1**, 259-270 (1990).
20. Cao, R.*, et al.* Role of histone H3 lysine 27 methylation in Polycomb-group silencing. *Science* **298**, 1039-1043 (2002).
21. Cao, R. & Zhang, Y. SUZ12 is required for both the histone methyltransferase activity and the silencing function of the EED-EZH2 complex. *Molecular cell* **15**, 57-67 (2004).
22. Simon, J.A. & Kingston, R.E. Mechanisms of polycomb gene silencing: knowns and unknowns. *Nature reviews. Molecular cell biology* **10**, 697-708 (2009).
23. Eich, M.L., Athar, M., Ferguson, J.E., 3rd & Varambally, S. EZH2-Targeted Therapies in Cancer: Hype or a Reality. *Cancer Res* **80**, 5449-5458 (2020).
24. Bachmann, I.M.*, et al.* EZH2 expression is associated with high proliferation rate and aggressive tumor subgroups in cutaneous melanoma and cancers of the endometrium, prostate, and breast. *Journal of clinical oncology : official journal of the American Society of Clinical Oncology* **24**, 268-273 (2006).
25. Bracken, A.P.*, et al.* EZH2 is downstream of the pRB-E2F pathway, essential for proliferation and amplified in cancer. *The EMBO journal* **22**, 5323-5335 (2003).
26. Fan, T.*, et al.* EZH2-dependent suppression of a cellular senescence phenotype in melanoma cells by inhibition of p21/CDKN1A expression. *Molecular cancer research : MCR* **9**, 418-429 (2011).
27. Zingg, D.*, et al.* EZH2-Mediated Primary Cilium Deconstruction Drives Metastatic Melanoma Formation. *Cancer Cell* **34**, 69-84 e14 (2018).
28. Zingg, D.*, et al.* The epigenetic modifier EZH2 controls melanoma growth and metastasis through silencing of distinct tumour suppressors. *Nature communications* **6**, 6051 (2015).
29. Tiffen, J., Wilson, S., Gallagher, S.J., Hersey, P. & Filipp, F.V. Somatic Copy Number Amplification and Hyperactivating Somatic Mutations of EZH2 Correlate With DNA Methylation and Drive Epigenetic Silencing of Genes Involved in Tumor Suppression and Immune Responses in Melanoma. *Neoplasia* **18**, 121-132 (2016).
30. Zingg, D.*, et al.* The Histone Methyltransferase Ezh2 Controls Mechanisms of Adaptive Resistance to Tumor Immunotherapy. *Cell Rep* **20**, 854-867 (2017).
31. Kim, K.H. & Roberts, C.W. Targeting EZH2 in cancer. *Nat Med* **22**, 128-134 (2016).
32. Rugo, H.S.*, et al.* The Promise for Histone Methyltransferase Inhibitors for Epigenetic Therapy in Clinical Oncology: A Narrative Review. *Advances in therapy* **37**, 3059-3082 (2020).
33. Duan, R., Du, W. & Guo, W. EZH2: a novel target for cancer treatment. *Journal of hematology & oncology* **13**, 104 (2020).
34. Huang, J.*, et al.* The noncanonical role of EZH2 in cancer. *Cancer Sci* **112**, 1376-1382 (2021).
35. Abali, G.K.*, et al.* EZH2 Abundance Regulated by UHRF1/UBE2L6/UBR4 Ubiquitin System is the Potential Therapeutic Target to Trigger Pigmented Phenotype in Melanoma. *bioRxiv*, 2021.2003.2004.433988 (2021).
36. Su, I.H.*, et al.* Polycomb group protein ezh2 controls actin polymerization and cell signaling. *Cell* **121**, 425-436 (2005).
37. Bryant, R.J., Winder, S.J., Cross, S.S., Hamdy, F.C. & Cunliffe, V.T. The Polycomb Group protein EZH2 regulates actin polymerization in human prostate cancer cells. *Prostate* **68**, 255-263 (2008).
38. Anwar, T.*, et al.* p38-mediated phosphorylation at T367 induces EZH2 cytoplasmic localization to promote breast cancer metastasis. *Nature communications* **9**, 2801 (2018).
39. Pang, J.*, et al.* Invasive breast carcinomas in Ghana: high frequency of high grade, basal-like histology and high EZH2 expression. *Breast Cancer Res Treat* **135**, 59-66 (2012).

40. Ahmad, F.*, et al.* Telomerase reverse transcriptase (TERT) - enhancer of zeste homolog 2 (EZH2) network regulates lipid metabolism and DNA damage responses in glioblastoma. *Journal of neurochemistry* **143**, 671-683 (2017).
41. Yiew, N.K.H.*, et al.* Enhancer of zeste homolog 2 (EZH2) regulates adipocyte lipid metabolism independent of adipogenic differentiation: Role of apolipoprotein E. *The Journal of biological chemistry* **294**, 8577-8591 (2019).
42. Behren, A.*, et al.* The Ludwig institute for cancer research Melbourne melanoma cell line panel. *Pigment Cell Melanoma Res* **26**, 597-600 (2013).
43. Kuser-Abali, G., Alptekin, A., Lewis, M., Garraway, I.P. & Cinar, B. YAP1 and AR interactions contribute to the switch from androgen-dependent to castration-resistant growth in prostate cancer. *Nature communications* **6**, 8126 (2015).
44. Livak, K.J. & Schmittgen, T.D. Analysis of relative gene expression data using real-time quantitative PCR and the 2(-Delta Delta C(T)) Method. *Methods* **25**, 402-408 (2001).
45. Dobin, A.*, et al.* STAR: ultrafast universal RNA-seq aligner. *Bioinformatics* **29**, 15-21 (2013).
46. Liao, Y., Smyth, G.K. & Shi, W. featureCounts: an efficient general purpose program for assigning sequence reads to genomic features. *Bioinformatics* **30**, 923-930 (2014).
47. Cerami, E.*, et al.* The cBio cancer genomics portal: an open platform for exploring multidimensional cancer genomics data. *Cancer Discov* **2**, 401-404 (2012).
48. Tyanova, S., Temu, T. & Cox, J. The MaxQuant computational platform for mass spectrometry-based shotgun proteomics. *Nat Protoc* **11**, 2301-2319 (2016).
49. Cox, J.*, et al.* Andromeda: a peptide search engine integrated into the MaxQuant environment. *J Proteome Res* **10**, 1794-1805 (2011).
50. Tyanova, S.*, et al.* The Perseus computational platform for comprehensive analysis of (prote)omics data. *Nat Methods* **13**, 731-740 (2016).
51. Shah, A.D., Goode, R.J.A., Huang, C., Powell, D.R. & Schittenhelm, R.B. LFQ-Analyst: An Easy-To-Use Interactive Web Platform To Analyze and Visualize Label-Free Proteomics Data Preprocessed with MaxQuant. *J Proteome Res* **19**, 204-211 (2020).
52. Gunter, J.H.*, et al.* Characterisation of inosine monophosphate dehydrogenase expression during retinal development: differences between variants and isoforms. *The international journal of biochemistry & cell biology* **40**, 1716-1728 (2008).
53. Benjanuwattra, J., Chaiyawat, P., Pruksakorn, D. & Koonrungsesomboon, N. Therapeutic potential and molecular mechanisms of mycophenolic acid as an anticancer agent. *Eur J Pharmacol* **887**, 173580 (2020).
54. Bentley, R. Mycophenolic Acid: a one hundred year odyssey from antibiotic to immunosuppressant. *Chem Rev* **100**, 3801-3826 (2000).
55. Drygin, D., Rice, W.G. & Grummt, I. The RNA polymerase I transcription machinery: an emerging target for the treatment of cancer. *Annu Rev Pharmacol Toxicol* **50**, 131-156 (2010).
56. Grummt, I. The nucleolus-guardian of cellular homeostasis and genome integrity. *Chromosoma* **122**, 487-497 (2013).
57. Pelletier, J., Thomas, G. & Volarevic, S. Ribosome biogenesis in cancer: new players and therapeutic avenues. *Nat Rev Cancer* **18**, 51-63 (2018).
58. Grummt, I. & Grummt, F. Control of nucleolar RNA synthesis by the intracellular pool sizes of ATP and GTP. *Cell* **7**, 447-453 (1976).
59. Huang, M. & Mitchell, B.S. Guanine nucleotide depletion mediates translocation of nucleolar proteins, including RNA helicase A (DHX-9). *Nucleosides Nucleotides Nucleic Acids* **27**, 704-711 (2008).
60. Orgaz, J.L., Herraiz, C. & Sanz-Moreno, V. Rho GTPases modulate malignant transformation of tumor cells. *Small GTPases* **5**, e29019 (2014).
61. Abrams, R. & Bentley, M. Biosynthesis of nucleic acid purines. II. Role of hypoxanthine and xanthine compounds. *Arch Biochem Biophys* **58**, 109-118 (1955).

62. Abrams, R. & Bentley, M. Biosynthesis of nucleic acid purines. I. Formation of guanine from adenine compounds in bone marrow extracts. *Arch Biochem Biophys* **56**, 184-195 (1955).
63. Lagerkvist, U., Reichard, P., Carlsson, B. & Grabosz, J. The biogenesis of pentosenucleic acid pyrimidines in the Ehrlich ascites tumor. *Cancer Res* **15**, 164-169 (1955).
64. Cheng, Y., Li, Y., Huang, X., Wei, W. & Qu, Y. Expression of EZH2 in uveal melanomas patients and associations with prognosis. *Oncotarget* **8**, 76423-76431 (2017).
65. Kleer, C.G.*, et al.* EZH2 is a marker of aggressive breast cancer and promotes neoplastic transformation of breast epithelial cells. *Proc Natl Acad Sci U S A* **100**, 11606-11611 (2003).
66. Xu, K.*, et al.* EZH2 oncogenic activity in castration-resistant prostate cancer cells is Polycomb-independent. *Science* **338**, 1465-1469 (2012).
67. Li, H., Cai, Q., Godwin, A.K. & Zhang, R. Enhancer of zeste homolog 2 promotes the proliferation and invasion of epithelial ovarian cancer cells. *Molecular cancer research : MCR* **8**, 1610-1618 (2010).
68. Terranova, C.J.*, et al.* Reprogramming of bivalent chromatin states in NRAS mutant melanoma suggests PRC2 inhibition as a therapeutic strategy. *Cell reports* **36**, 109410 (2021).
69. Schoumacher, M.*, et al.* Uveal melanoma cells are resistant to EZH2 inhibition regardless of BAP1 status. *Nature medicine* **22**, 577-578 (2016).
70. Jin, B.*, et al.* Verification of EZH2 as a druggable target in metastatic uveal melanoma. *Molecular cancer* **19**, 52 (2020).
71. Kim, W.*, et al.* Targeted disruption of the EZH2-EED complex inhibits EZH2-dependent cancer. *Nature chemical biology* **9**, 643-650 (2013).
72. Gunawan, M.*, et al.* The methyltransferase Ezh2 controls cell adhesion and migration through direct methylation of the extranuclear regulatory protein talin. *Nature immunology* **16**, 505-516 (2015).
73. Cornuel, J.F., Moraillon, A. & Gueron, M. Participation of yeast inosine 5'-monophosphate dehydrogenase in an in vitro complex with a fragment of the C-rich telomeric strand. *Biochimie* **84**, 279-289 (2002).
74. McLean, J.E.*, et al.* Inosine 5'-monophosphate dehydrogenase binds nucleic acids in vitro and in vivo. *Biochem J* **379**, 243-251 (2004).
75. Mortimer, S.E. & Hedstrom, L. Autosomal dominant retinitis pigmentosa mutations in inosine 5'-monophosphate dehydrogenase type I disrupt nucleic acid binding. *Biochem J* **390**, 41-47 (2005).
76. Bowne, S.J.*, et al.* Spectrum and frequency of mutations in IMPDH1 associated with autosomal dominant retinitis pigmentosa and leber congenital amaurosis. *Invest Ophthalmol Vis Sci* **47**, 34-42 (2006).
77. Kozhevnikova, E.N.*, et al.* Metabolic enzyme IMPDH is also a transcription factor regulated by cellular state. *Molecular cell* **47**, 133-139 (2012).
78. Chang, T.S., Chao, S.Y. & Ding, H.Y. Melanogenesis inhibition by homoisoflavavone sappanone A from Caesalpinia sappan. *Int J Mol Sci* **13**, 10359-10367 (2012).
79. Liebhaber, S.A., Wolf, S. & Schlessinger, D. Differences in rRNA metabolism of primary and SV40-transformed human fibroblasts. *Cell* **13**, 121-127 (1978).
80. Kauffmann, A.*, et al.* High expression of DNA repair pathways is associated with metastasis in melanoma patients. *Oncogene* **27**, 565-573 (2008).
81. Jayaram, H.N., Cooney, D.A., Grusch, M. & Krupitza, G. Consequences of IMP dehydrogenase inhibition, and its relationship to cancer and apoptosis. *Curr Med Chem* **6**, 561-574 (1999).
82. Wright, D.G.*, et al.* Tiazofurin effects on IMP-dehydrogenase activity and expression in the leukemia cells of patients with CML blast crisis. *Anticancer Res* **16**, 3349-3351 (1996).
83. Carter, S.B.*, et al.* Mycophenolic acid: an anti-cancer compound with unusual properties. *Nature* **223**, 848-850 (1969).
84. Sweeney, M.J.*, et al.* Experimental antitumor activity and preclinical toxicology of mycophenolic acid. *Cancer Res* **32**, 1795-1802 (1972).

85. Naffouje, R.*, et al.* Anti-Tumor Potential of IMP Dehydrogenase Inhibitors: A Century-Long Story. *Cancers* **11**(2019).
86. Sobiak, J., Kaminska, J., Glyda, M., Duda, G. & Chrzanowska, M. Effect of mycophenolate mofetil on hematological side effects incidence in renal transplant recipients. *Clin Transplant* **27**, E407-414 (2013).
87. Staatz, C.E. & Tett, S.E. Pharmacology and toxicology of mycophenolate in organ transplant recipients: an update. *Arch Toxicol* **88**, 1351-1389 (2014).
88. Bremer, S.*, et al.* Expression of IMPDH1 and IMPDH2 after transplantation and initiation of immunosuppression. *Transplantation* **85**, 55-61 (2008).
89. Jonsson, C.A. & Carlsten, H. Mycophenolic acid inhibits inosine 5'-monophosphate dehydrogenase and suppresses immunoglobulin and cytokine production of B cells. *Int Immunopharmacol* **3**, 31-37 (2003).
90. Huang, F.*, et al.* Inosine Monophosphate Dehydrogenase Dependence in a Subset of Small Cell Lung Cancers. *Cell Metab* **28**, 369-382 e365 (2018).
91. Liu, Y.C.*, et al.* Global regulation of nucleotide biosynthetic genes by c-Myc. *PLoS One* **3**, e2722 (2008).
92. Karigane, D.*, et al.* p38alpha Activates Purine Metabolism to Initiate Hematopoietic Stem/Progenitor Cell Cycling in Response to Stress. *Cell Stem Cell* **19**, 192-204 (2016).
93. Cantelli, G.*, et al.* TGF-beta-Induced Transcription Sustains Amoeboid Melanoma Migration and Dissemination. *Curr Biol* **25**, 2899-2914 (2015).

Figure Legends

Figure 1. Methylation-independent functions of EZH2 are predominant in melanoma. A375 cells were treated with siEZH2, 2 μM DZNep, 2 μM GSK126, 2 μM EPZ6438 and scramble or DMSO (control) for 3 days prior to: (A) Western blot analysis of EZH2, H3K27me3, H3 and β-Actin protein level, (B) cell growth analysis done by Trypan Blue haemocytometer counting, (C) clonogenicity after low-density seeding (crystal violet stain). Clonogenicity was assessed in pre-treated (3 days) cells seeded at 2000 cells in 6-well plate followed by crystal violet staining (0.5% in methanol) after incubation for 10 days in drug-free media. Representative images after crystal violet-stained wells were shown above bars (D) Boyden chamber migration was assessed in pre-treated (3 days) cells seeded at 50,000 cells in 24-well plate after incubation for 24h. Representative images after crystal violet-stained wells were shown above bars. (E) B16-F10 cells were treated with either GSK126 versus vehicle control (DMSO) or siEzh2 versus siCtrl and then profiled in triplicate RNAseq experiments. Genes that were significantly up- or downregulated by siEzh2 compared with the control were clustered across all samples and are shown as heatmaps. Each row represents one gene and each column triplicate sample. The siEzh2-induced genes that were also induced by GSK126 were termed class I genes and those unchanged by GSK126 class II genes. Genes that were activated by Ezh2 were defined as class III genes. (F) Venn diagram showing overlap among si-Ezh2 induced and GSK126-induced genes compiled from RNAseq experiment in G. (G) GO biological process analysis of 1226 class II genes. (H) Venn diagram showing overlap among si-Ezh2 repressed and GSK126-repressed genes compiled from RNAseq experiment in G. (I) GO biological process analysis of 1087 class III genes. Data for B-D are from three independent experiments and are presented as mean ±SD. ns: non-significant; * $p < 0.01$; ** $p \leq 0.01$; ***$p \leq 0.005$.

Figure 2. EZH2 has methyltransferase independent function in melanoma tumorigenicity and invasion. (A) Western blot analysis of A375 cells showing EZH2 knockdown after lentiviral transduction with control shRNA (shControl) or 3′ UTR EZH2-targeting shRNA (shEZH2) and rescue with V5-tagged WT-EZH2 or methyltransferase deficient H689A-EZH2. (B) Clonogenicity assay of cells described in A. Representative images after crystal violet-stained wells were shown above bars. (C) Matrigel-coated Boyden chamber invasion assay of cells described in A.

Representative images after crystal violet staining were shown above bars. (D) Wound healing assay of cells described in A. Representative images of the wound after 24 h shown above bars. (E) Tumor caliper of A375 xenografts as described in A. (F) Tumor weights of A375 xenografts at the end point. Representative tumors per group were shown above bars. (G) V5-EZH2 deletion mutant constructs. (H) Western blot analysis, (I) invasion, (J) clonogenicity of A375 cells with EZH2 knockdown followed by rescue with V5-tagged EZH2 deletion mutant vectors. Data for B-D, I, J are from at least three independent experiments and are presented as mean ±SD. *p ≤ 0.05, **p ≤ 0.01. Data for E, F are from 7 mice per group and are presented as mean ±SD. ns: non-significant, *p ≤ 0.05, **p ≤ 0.01, ***p ≤ 0.005.

Figure 3. Cytosolic EZH2 interacts with IMPDH2 through the IMPDH2-CBS domain and moves IMPDH2 to cytoplasm/ increases its tetramerization. A) List of overlapping proteins co-immunoprecipitated (Co-IP) with EZH2 from C006-M1, LM-MEL-28:B4:F3, IGR37, A375 and LM-MEL-45 melanoma cells (all data derived from n=3 biological replicates). (B) The interaction between endogenous EZH2 and IMPDH2 was determined in A375 cells by immunoprecipitation (IP) with anti-IMPDH2 and anti-EZH2 antibody followed by western blotting with anti-EZH2 and anti-IMPDH2 antibody. (C) HA-tagged EZH2-WT and V5-tagged IMPDH2 (1-187) were co-expressed in A375 cells. The interaction between overexpressed EZH2 and IMPDH2 (1-187) was determined by immunoprecipitation with anti-HA antibody followed by western blotting with anti-V5 antibody. (D) GST-EZH2 deletion mutant constructs. (E) The binding of V5-IMPDH2-CBS protein to GST–EZH2 peptides was probed with WB using the V5 specific antibody. Total cell lysate from HEK293 overexpressing V5-IMPDH2-CBS was used as a source of IMPDH2-CBS in GST–pull-down experiment. (F) The binding of Myc/Flag tagged full length IMPDH2 protein to V5 tagged EZH2 deletion mutant peptides (shown in Fig. 2G) was shown by co-IP with anti-Flag antibody followed by probing with anti-V5 antibody. (G) Ligation proximity images depicting co-localization with EZH2 and IMPDH2 by red fluorescent dots A375 cells. Scale bar=10 μm. Number of interaction loci depicted as red dots were counted for cytoplasm and nucleus of total of 100 cell. (H) Cytosolic/Nuclear fractionation was done for A375, B4:F3, IGR37, B16-F10 cells followed by IP with anti-EZH2 antibody followed by western blotting with anti-EZH2 and anti-IMPDH2 antibody (right). Lamin A/C is nuclear, and β-Actin is cytosolic marker. Inputs were shown on the left. (I)

Matrigel-coated Boyden chamber invasion assay of A375 cells showing EZH2 knockdown after lentiviral transduction with control shRNA (shControl) or 3′ UTR EZH2-targeting shRNA (shEZH2) and rescue with V5-WT-EZH2 or V5-EZH2-H689A, V5-EZH2-ΔNLS-WT and V5-EZH2-ΔNLS-H689A. Representative images after crystal violet staining were shown above bars. (J) Tumor weights of indicated A375 xenografts (n=7) at the end point. (K) Cytosolic/Nuclear fractionation was done from A375 cells with control shRNA (shControl) or 3′ UTR EZH2-targeting shRNA followed by IP with anti-EZH2 antibody followed by western blotting with anti-EZH2 and anti-IMPDH2 antibody. Lamin A/C is nuclear, and β-Actin is cytosolic marker. (L) Cytosolic/Nuclear fractionation was done from cells described in (I) followed by western blotting with anti-V5, anti-EZH2, anti-IMPDH2 antibody and β-Actin antibody. (M) The clusters of IMPDH2 and IMPDH1 tetramer were detected from cross-linked whole-cell extracts isolated from cells described in Figure 2A. Data for I is from three independent experiments and are presented as mean ±SD. ns: non-significant, * $p< 0.01$, ** $p< 0.001$, *** $p< 0.0001$.

Figure 4. IMPDH2 induces clonogenecity/ invasion in melanoma cells by regulating ribosome biogenesis and actomyosin contractility via cellular GTP level regulation. (A) Time-dependent growth curves of A375 cells upon 25 μM Ribavirin or DMSO (control); 3 μM MPA, or methanol (Control). (B) A375 cell growth analysis done by Trypan Blue haemocytometer counting after treated with 3 μM MPA or methanol control with the addition of 100 μM guanosine or vehicle control for 3 days. (C) Clonogenicity assay of A375 cells described in A. Clonogenicity was assessed in pre-treated (2 and 3 days) cells seeded at 2000 cells in 6-well plate followed by crystal violet staining (0.5% in methanol) after incubation for 10 days in drug-free media. Representative images after crystal violet-stained wells were shown. (D) 3D matrigel clonogenicity assay of A375 and B16-F10 cells treated with 3 μM MPA or methanol (control) for 10 days. (E) Matrigel-coated Boyden chamber invasion assay of cells described in B. (F) Cell growth analysis done by Trypan Blue haemocytometer counting after A375 cells were treated with siIMPDH2 or scramble control with the addition of 100 μM guanosine or vehicle control for 3 days. (G) Matrigel-coated Boyden chamber invasion assay of cells described in F. (H) Nascent transcripts of the indicated genes were analyzed by qRT-PCR after A375 cells were treated with 3 μM MPA for 0h, 4h and 8h. (I) IF staining with anti-NCL antibody in A375 cells treated with

25 μM Ribavirin, 3 μM MPA, or methanol (Control) with the addition of 100 μM guanosine or vehicle control for 24h. DAPI stains the nuclei. Scale bar: 20 μm (J) RhoA activity assay in A375 cells treated with 3 μM MPA or methanol (Control) with the addition of 100 μM guanosine for 24h. (K) IF staining of A375 cells described in J with anti-p-MLC2 (green) and phalloidin (red). DAPI stains the nuclei. Scale bar: 20 μm. % peripheral p-MLC2 positive cells were plotted on the right plot. Data for A, B, F, H, J and K are from three independent experiments and are presented as mean ±SD. ns: non-significant, * p< 0.01, ** p< 0.001, *** p< 0.0001.

Figure 5. EZH2 regulates clonogenicity/invasion by regulating rRNA metabolism and Rho GTPase activity via GTP production in melanoma. (A) Relative GTP levels were quantified by HPLC in A375 cells with stable EZH2 knockdown (shEZH2) and overexpression with V5-EZH2-clone2. (B) Cell growth analysis of A375 cells with stable EZH2 knockdown after 3 days of control or 100 μM guanosine addition done by Trypan Blue haemocytometer counting. (C) Cell growth analysis done by Trypan Blue haemocytometer counting and (D) invasion assay counting done by crystal violet staining after A375 cells with stable EZH2 knockdown were rescued by V5-tagged WT-EZH2 or methyltransferase deficient H689A-EZH2 overexpression followed by scramble, si-IMPDH2#1, or si-IMPDH2#2 oligos and 100 μM guanosine addition. (E) Nascent transcripts of the indicated genes were analyzed by qRT-PCR, (F) RhoA activity assay, (G) p-MLC2 IF in A375 cells showing EZH2 knockdown after lentiviral transduction with control shRNA (shControl) or 3′ UTR EZH2-targeting shRNA (shEZH2) and rescue with V5-tagged WT-EZH2 or methyltransferase deficient H689A-EZH2. % Peripheral p-MLC2 positive cells were plotted below images. (H) % peripheral p-MLC2 positive cells were plotted. (I) Human melanoma samples from grade I to IV were stained with anti-EZH2 and anti-IMPDH2 antibodies. Grade I, II, III: n=31 grade IV: n=8. Nucleolar sizes were measured from HE stained samples. Scale bar: 50 μm. Data for A-I are from three independent experiments and are presented as mean ±SD. * p< 0.01, ** p< 0.001, *** p< 0.0001.

Figure 6. Pharmacological inhibition of EZH2/IMPDH2 interaction by SA attenuates the growth and invasion abilities of melanoma cells *in vitro*. (A) The interaction between endogenous EZH2 and IMPDH2 upon 16h SA treatment (DMSO, 5, 10, 20 μM) was determined in A375 cells by IP with anti-EZH2 antibody followed by WB with anti-EZH2 and anti-IMPDH2 antibody. The inputs were shown on the left. (B)

The interaction between HA-EZH2 and V5-IMPDH2-CBS upon 16h SA treatment (DMSO, 2, 5, 10 μM) was determined in A375 cells by IP with anti-HA antibody followed by WB with anti-V5 and anti-HA antibody. The inputs were shown above the IP blots. (C) The clusters of IMPDH2 tetramer were detected from cross-linked whole-cell extracts isolated from A375 cells treated with SA for 16h. (D) Cytosolic versus nuclear localizations of EZH2 and IMPDH2 were examined upon SA treatment in A375 cells by Co-IF using anti-EZH2 (green) and anti-IMPDH2 (red) antibodies. DAPI stains the nuclei. Scale bar: 20 μm. % nuclear IMPDH2 positive cells were plotted for each group. (E) Dose dependent cell growth curve of A375 cells treated with the indicated dose of SA and -/+ 100 μM guanosine for 3 days. Clonogenicity was shown in the inlet. (F) Matrigel-coated Boyden chamber invasion assay in A375 cells with stable EZH2 knockdown and later rescued by V5-tagged WT-EZH2 overexpression followed by scramble, si-IMPDH2#1, or si-IMPDH2#2 oligos and 100 μM guanosine addition. (left), invaded cell numbers per field were plotted on the right graph. (G) Spheroid areas of 3D colonies grown for 4, 10, 14 days with DMSO or 5 μM SA containing culture medium were measured by Image J program. (H) Sphere formation in 3D Matrigel (preventive). A375 cells were grown in Matrigel for 10 days in presence of either DMSO (control) or 10 μM SA and then the colonies were grown 7 more days without SA or DMSO and spheres were counted manually and presented in the graph (I). (J) Sphere formation in 3D Matrigel (therapeutic). A375 cells were grown in Matrigel for 6 days in the absence of SA followed by 4d and 10d days with DMSO or 10 μM SA. Spheroid areas were measured by Image J program and presented in the graph (K). Invasive spheroid numbers were counted manually and presented in the graph (L). (M) The effect of SA on ribosome biogenesis was measured in A375 cells treated with the indicated doses of SA by anti-NCL antibody. DAPI stains the nuclei. Scale bar: 20 μm. (N) The effect of SA on EZH2 and IMPDH2 interaction was shown by Co-IP coupled WB in $CD34^+$ BM cells. Cell growth analysis of CD34+ bone marrow progenitor cells (O) and normal human melanocytes (P) treated with DMSO (vehicle), 2 μM, or 5 μM SA for the indicated time points. Data for D, E, F, G, I, K, L, M and O are from three independent experiments and are presented as mean ±SD. ns: non-significant, * $p< 0.01$, ** $p< 0.001$, *** $p< 0.0001$.

Figure 7. EZH2-IMPDH2 interaction is commonly seen in uveal melanoma, breast, prostate, ovarian cancer, and SA attenuates their growth in *vitro*. EZH2

and IMPDH2 interaction was shown by IP with anti-IMPDH2 antibody followed by WB with anti-EZH2 and anti-IMPDH2 antibody in (A) uveal melanoma, (B) ovarian cancer, (C) breast cancer and (D) prostate cancer cell lines. Inputs were shown at the top of each Co-IP blots. (E) Cytosolic/Nuclear fractionation was done for MDA-MB-231, C4-2, PC3, OVCAR8 and OMM1cells followed by IP with anti-EZH2 antibody followed by western blotting with anti-EZH2 and anti-IMPDH2 antibody. The effect of SA on EZH2 and IMPDH2 interaction was shown by Co-IP coupled WB in (F) OMM1 and (G) OVCAR8 cells. Dose-dependent growth curves of (H) OMM1, (I) OVCAR8, (J) MDA-MB-231 and (K) C4:2 cells upon SA treatment for 3 days. (L) Proposed model depicting both canonical nuclear and non-canonical cytosolic functions of EZH2 as an epigenetic silencer and as GTP regulator via IMPDH2 interaction, which can be blocked by SA. EZH2 induces tumorigenicity and metastasis in melanoma by upregulating rRNA metabolism and RhoA dependent actomyosin contractility via GTP production.

Figure1.

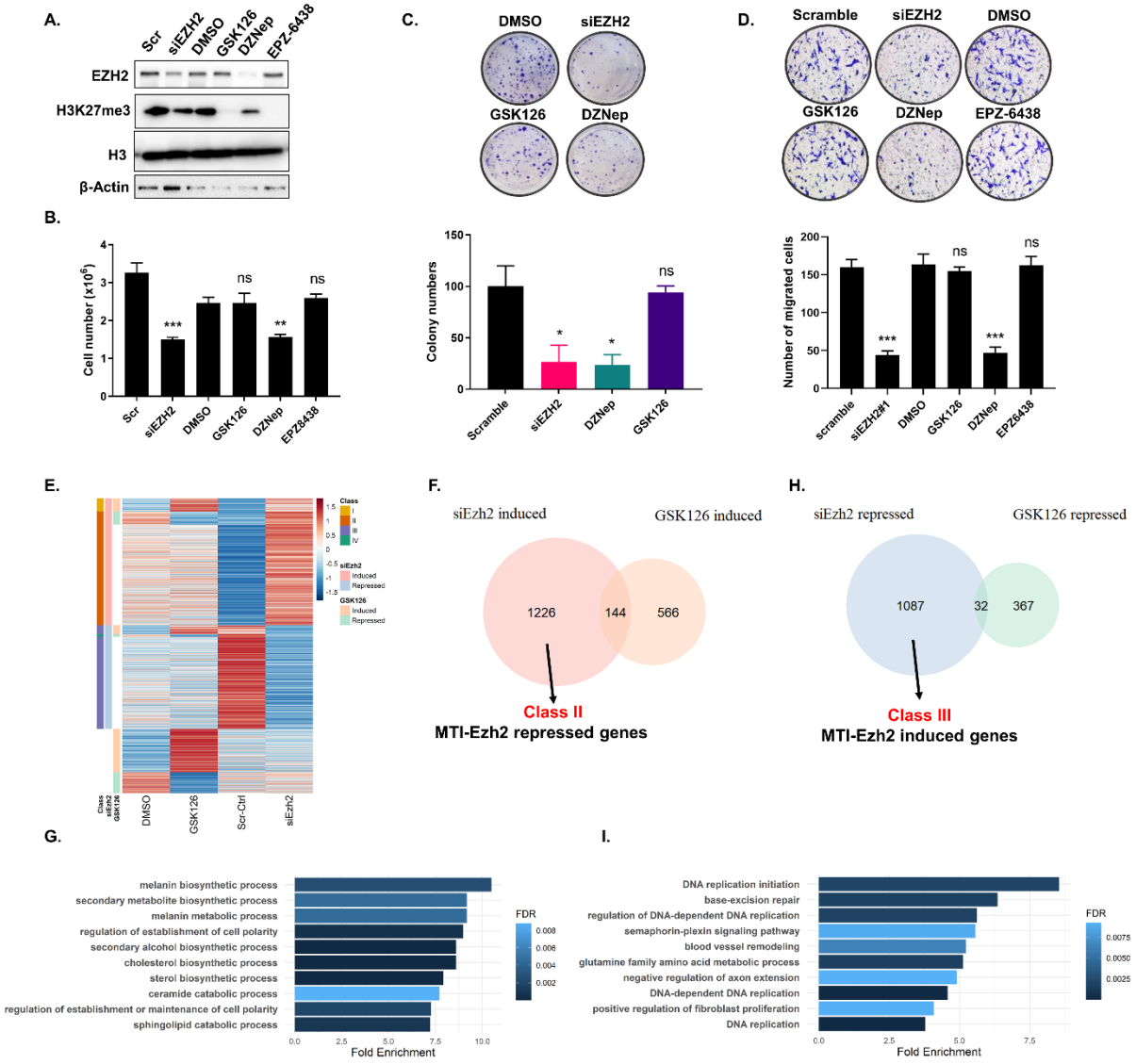
A.
Scr
siEZH2
DMSO
GSK126
DZNep
EPZ-6438
EZH2
H3K27me3
H3
β-Actin
B.
Cell number (x10^6)
ns
***
**
C.
DMSO
siEZH2
GSK126
DZNep
Colony numbers
D.
Scramble
siEZH2
DMSO
GSK126
DZNep
EPZ-6438
Number of migrated cells
siEZH2#1
E.
Class
siEzh2
Induced
Repressed
GSK126
F.
siEzh2 induced
GSK126 induced
1226
144
566
Class II
MTI-Ezh2 repressed genes
H.
siEzh2 repressed
GSK126 repressed
1087
32
367
Class III
MTI-Ezh2 induced genes
G.
melanin biosynthetic process
secondary metabolite biosynthetic process
melanin metabolic process
regulation of establishment of cell polarity
secondary alcohol biosynthetic process
cholesterol biosynthetic process
sterol biosynthetic process
ceramide catabolic process
regulation of establishment or maintenance of cell polarity
sphingolipid catabolic process
FDR
Fold Enrichment
I.
DNA replication initiation
base-excision repair
regulation of DNA-dependent DNA replication
semaphorin-plexin signaling pathway
blood vessel remodeling
glutamine family amino acid metabolic process
negative regulation of axon extension
DNA-dependent DNA replication
positive regulation of fibroblast proliferation
DNA replication
FDR
Fold Enrichment

Figure 2.

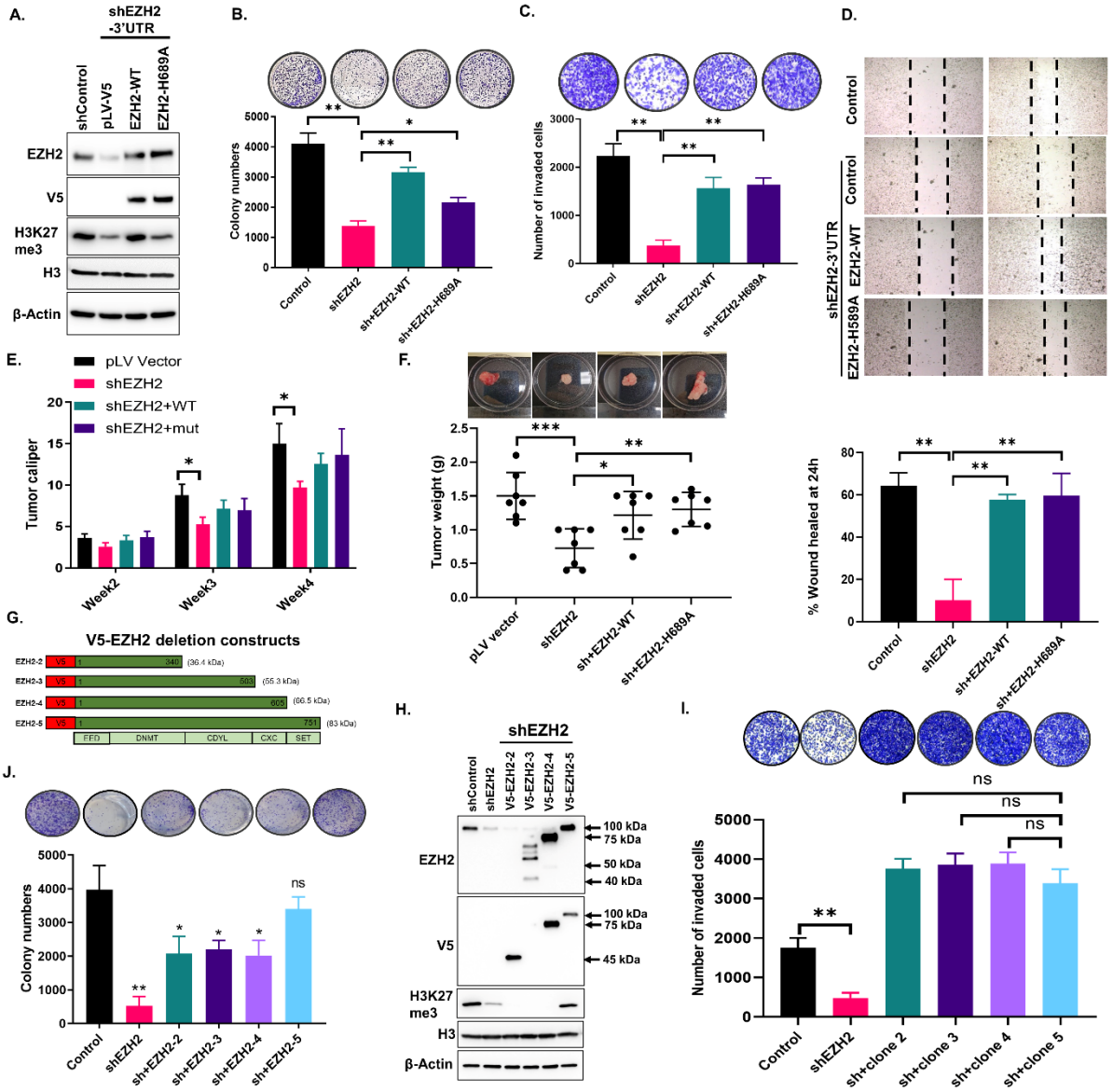
A.
shEZH2 -3'UTR
shControl
pLV-V5
EZH2-WT
EZH2-H689A
EZH2
V5
H3K27 me3
H3
β-Actin
B.
Colony numbers
Control
shEZH2
sh+EZH2-WT
sh+EZH2-H689A
C.
Number of invaded cells
D.
Control
shEZH2-3'UTR
EZH2-WT
EZH2-H589A
E.
pLV Vector
shEZH2
shEZH2+WT
shEZH2+mut
Tumor caliper
Week2
Week3
Week4
F.
Tumor weight (g)
pLV vector
% Wound healed at 24h
G.
V5-EZH2 deletion constructs
EZH2-2
EZH2-3
EZH2-4
EZH2-5
FFD
DNMT
CDYL
CXC
SET
H.
shEZH2
shControl
shEZH2
V5-EZH2-2
V5-EZH2-3
V5-EZH2-4
V5-EZH2-5
100 kDa
75 kDa
50 kDa
40 kDa
45 kDa
I.
Number of invaded cells
sh+clone 2
sh+clone 3
sh+clone 4
sh+clone 5
J.
Colony numbers
sh+EZH2-2
sh+EZH2-3
sh+EZH2-4
sh+EZH2-5
ns

Figure 3.

A.

Common EZH2 Interactors in Melanoma Cells			
PRC1/2 Complex	Kinesin 1 Complex	Nucleotide Metabolism	Ubiquitin Degradation
EED	KIF5B	IMPDH2	UBR4
SUZ12	KLC1		NPLOC4
JARID2	KLC2		
AEBP2	KLC4		
MTF2			
PHF1			
RBBP4			

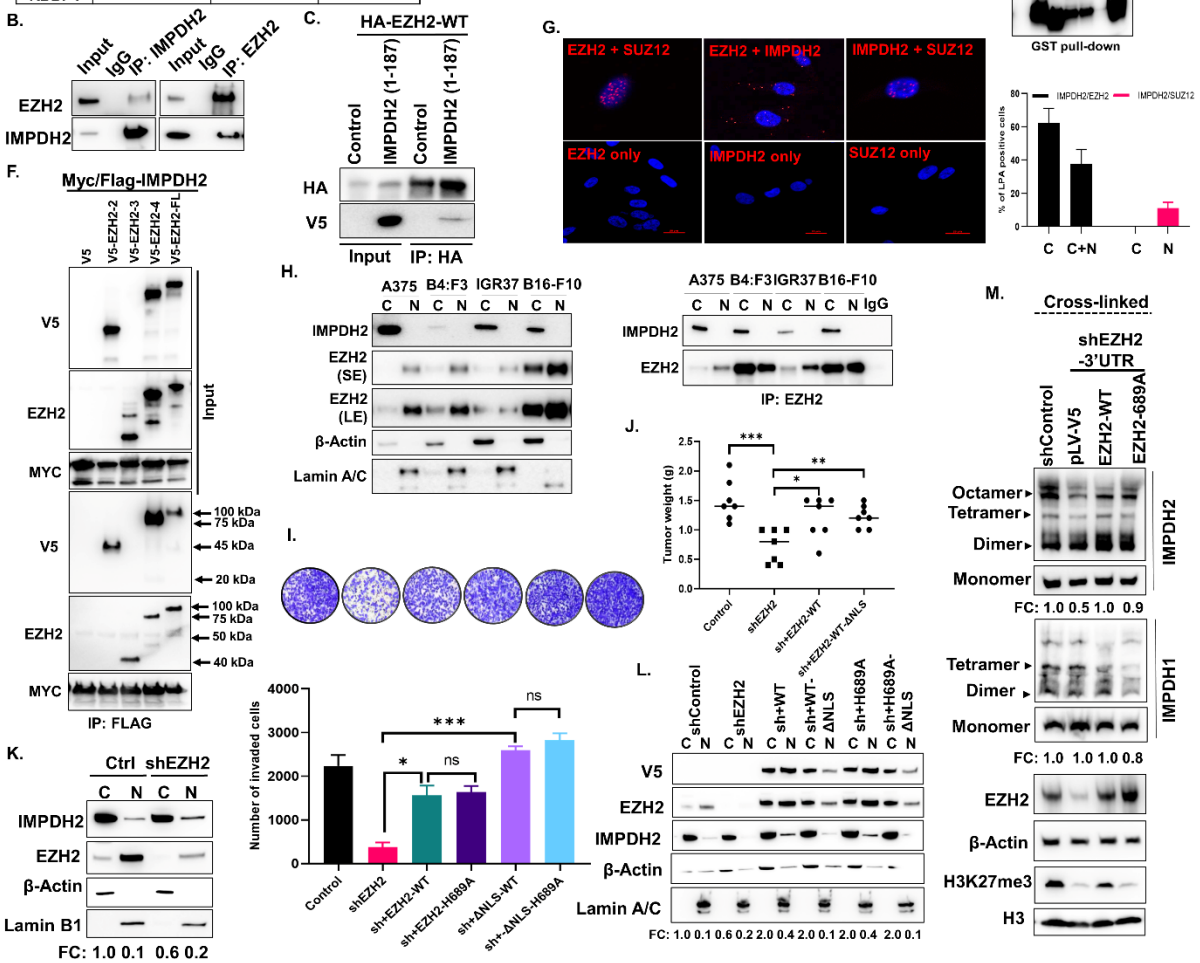

Figure 4.

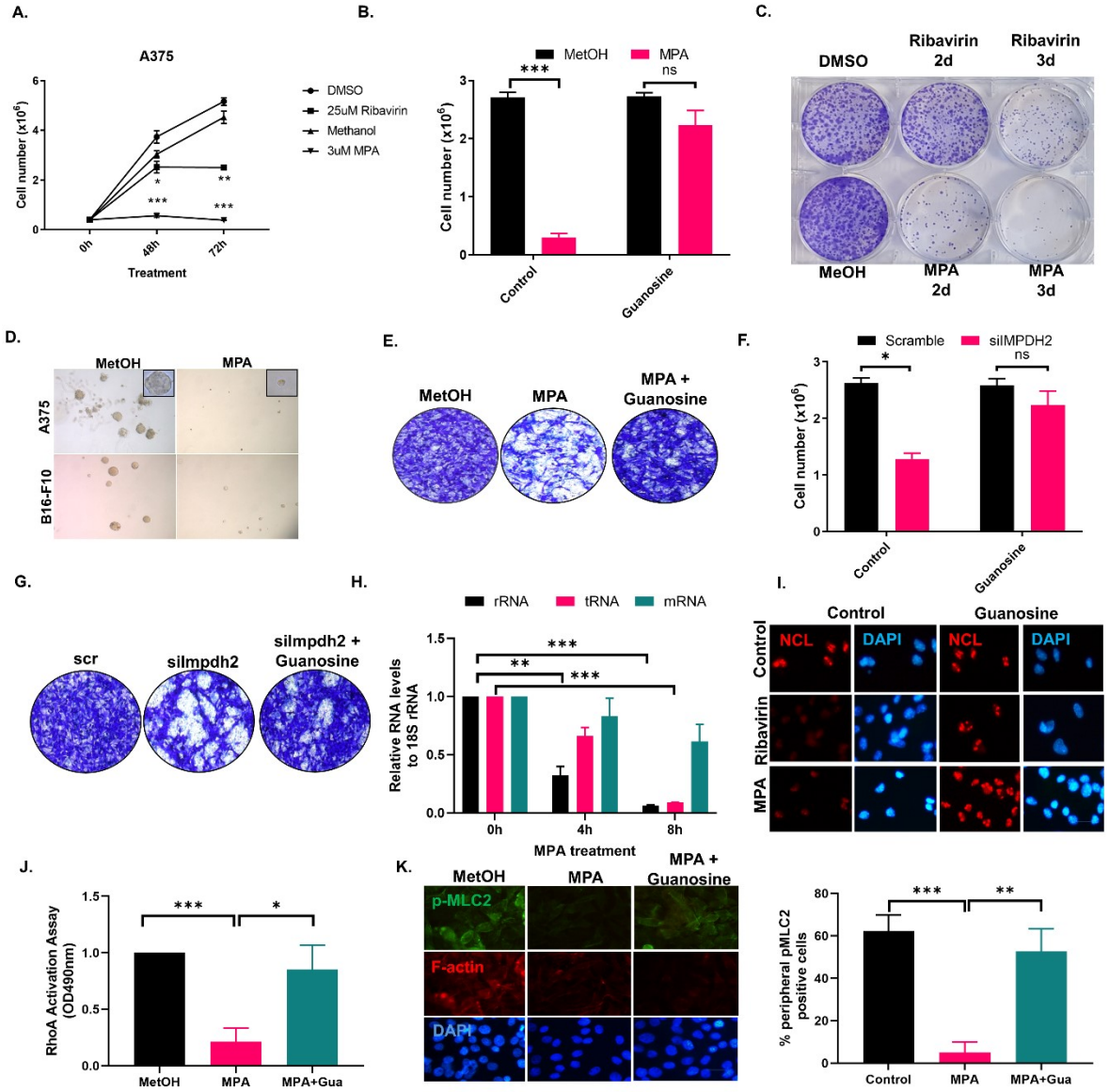
A.
A375
Cell number (x10^6)
Treatment
0h
48h
72h
DMSO
25uM Ribavirin
Methanol
3uM MPA
B.
MetOH
MPA
ns
Cell number (x10^6)
Control
Guanosine
C.
DMSO
Ribavirin 2d
Ribavirin 3d
MeOH
MPA 2d
MPA 3d
D.
MetOH
MPA
A375
B16-F10
E.
MetOH
MPA
MPA + Guanosine
F.
Scramble
siMPDH2
ns
Cell number (x10^6)
Control
Guanosine
G.
scr
siMPDH2
siMPDH2 + Guanosine
H.
rRNA
tRNA
mRNA
Relative RNA levels to 18S rRNA
0h
4h
8h
MPA treatment
I.
Control
Guanosine
NCL
DAPI
Control
Ribavirin
MPA
J.
RhoA Activation Assay (OD490nm)
MetOH
MPA
MPA+Gua
K.
MetOH
MPA
MPA + Guanosine
p-MLC2
F-actin
DAPI
% peripheral pMLC2 positive cells
Control
MPA
MPA+Gua

Figure 5.

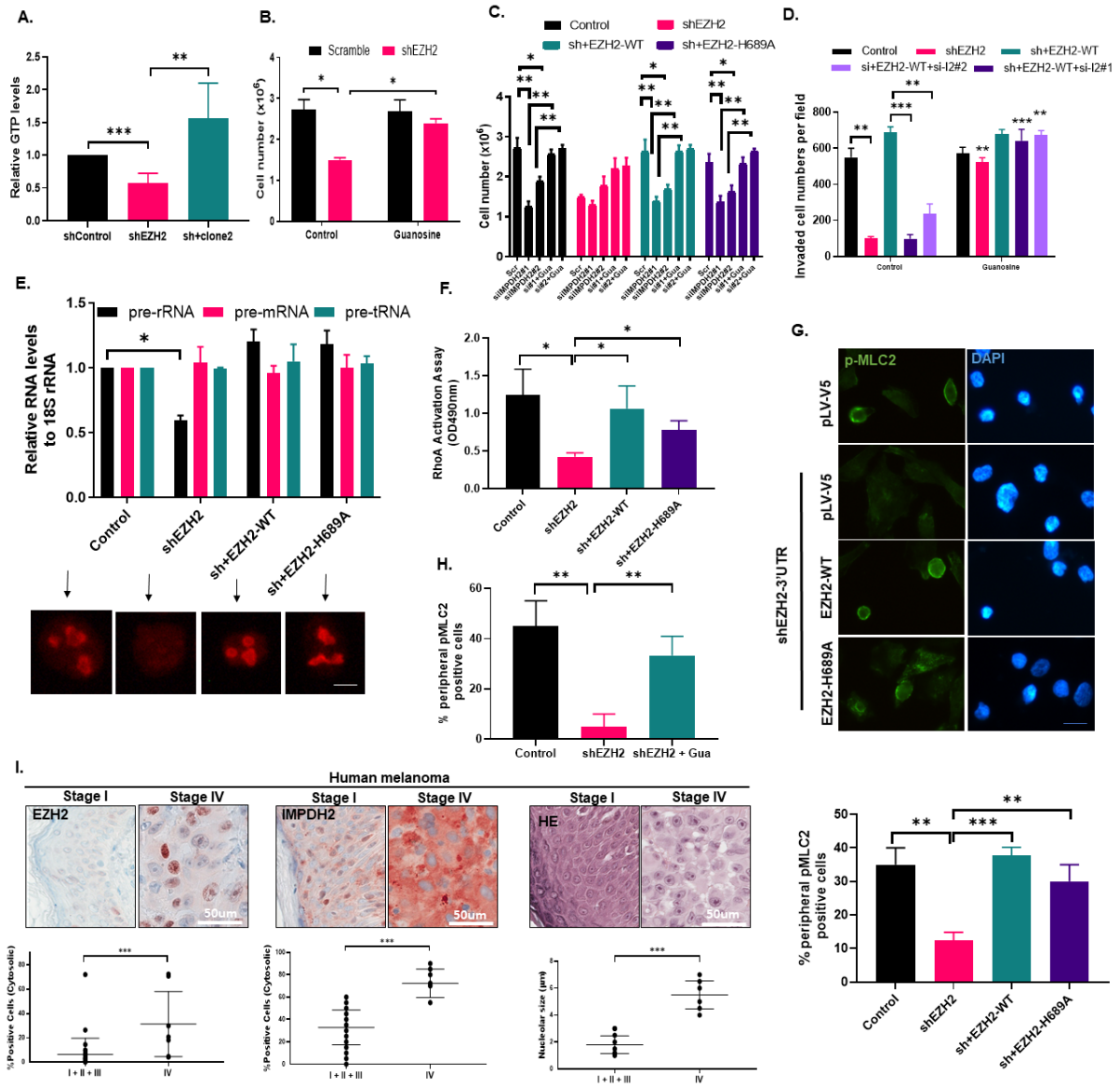
A.
Relative GTP levels
shControl
shEZH2
sh+clone2
B.
Scramble
shEZH2
Cell number (x10^6)
Control
Guanosine
C.
Control
shEZH2
sh+EZH2-WT
sh+EZH2-H689A
Cell number (x10^6)
D.
Control
shEZH2
sh+EZH2-WT
si+EZH2-WT+si-I2#2
sh+EZH2-WT+si-I2#1
Invaded cell numbers per field
Control
Guanosine
E.
pre-rRNA
pre-mRNA
pre-tRNA
Relative RNA levels to 18S rRNA
Control
shEZH2
sh+EZH2-WT
sh+EZH2-H689A
F.
RhoA Activation Assay (OD490nm)
Control
shEZH2
sh+EZH2-WT
sh+EZH2-H689A
G.
p-MLC2
DAPI
pLV-V5
pLV-V5
EZH2-WT
EZH2-H689A
shEZH2-3'UTR
H.
% peripheral pMLC2 positive cells
Control
shEZH2
shEZH2 + Gua
I.
Human melanoma
Stage I
Stage IV
EZH2
IMPDH2
HE
50um
% Positive Cells (Cytosolic)
Nucleolar size (μm)
I + II + III
IV
% peripheral pMLC2 positive cells
Control
shEZH2
sh+EZH2-WT
sh+EZH2-H689A

Figure 6.

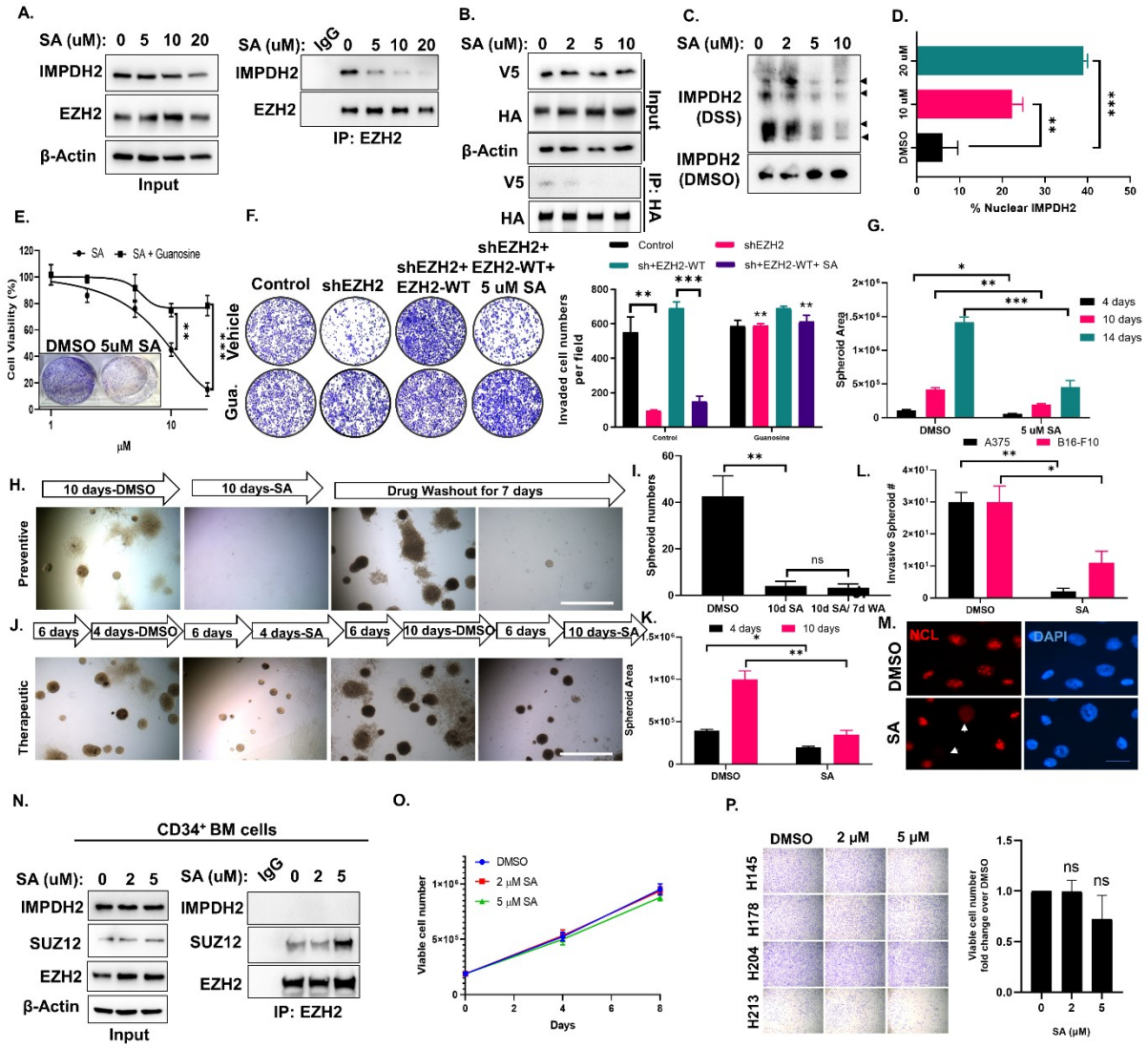
A.
SA (uM): 0 5 10 20
IMPDH2
EZH2
β-Actin
Input
SA (uM): IgG 0 5 10 20
IMPDH2
EZH2
IP: EZH2
B.
SA (uM): 0 2 5 10
V5
HA
β-Actin
Input
V5
HA
IP: HA
C.
SA (uM): 0 2 5 10
IMPDH2 (DSS)
IMPDH2 (DMSO)
D.
DMSO
10 uM
20 uM
% Nuclear IMPDH2
E.
SA
SA + Guanosine
Cell Viability (%)
DMSO 5uM SA
μM
F.
Control
shEZH2
shEZH2+ EZH2-WT
shEZH2+ EZH2-WT+ 5 uM SA
Vehicle
Gua.
Control
shEZH2
sh+EZH2-WT
sh+EZH2-WT+ SA
Invaded cell numbers per field
Control
Guanosine
G.
4 days
10 days
14 days
Spheroid Area
DMSO
5 uM SA
A375
B16-F10
H.
10 days-DMSO
10 days-SA
Drug Washout for 7 days
Preventive
I.
Spheroid numbers
DMSO
10d SA
10d SA/ 7d WA
L.
Invasive Spheroid #
DMSO
SA
J.
6 days
4 days-DMSO
6 days
4 days-SA
6 days
10 days-DMSO
6 days
10 days-SA
Therapeutic
K.
4 days
10 days
Spheroid Area
DMSO
SA
M.
NCL
DAPI
DMSO
SA
N.
CD34+ BM cells
SA (uM): 0 2 5
IMPDH2
SUZ12
EZH2
β-Actin
Input
SA (uM): IgG 0 2 5
IMPDH2
SUZ12
EZH2
IP: EZH2
O.
DMSO
2 μM SA
5 μM SA
Viable cell number
Days
P.
DMSO
2 μM
5 μM
H145
H178
H204
H213
Viable cell number fold change over DMSO
ns
ns
SA (μM)

Figure 7.

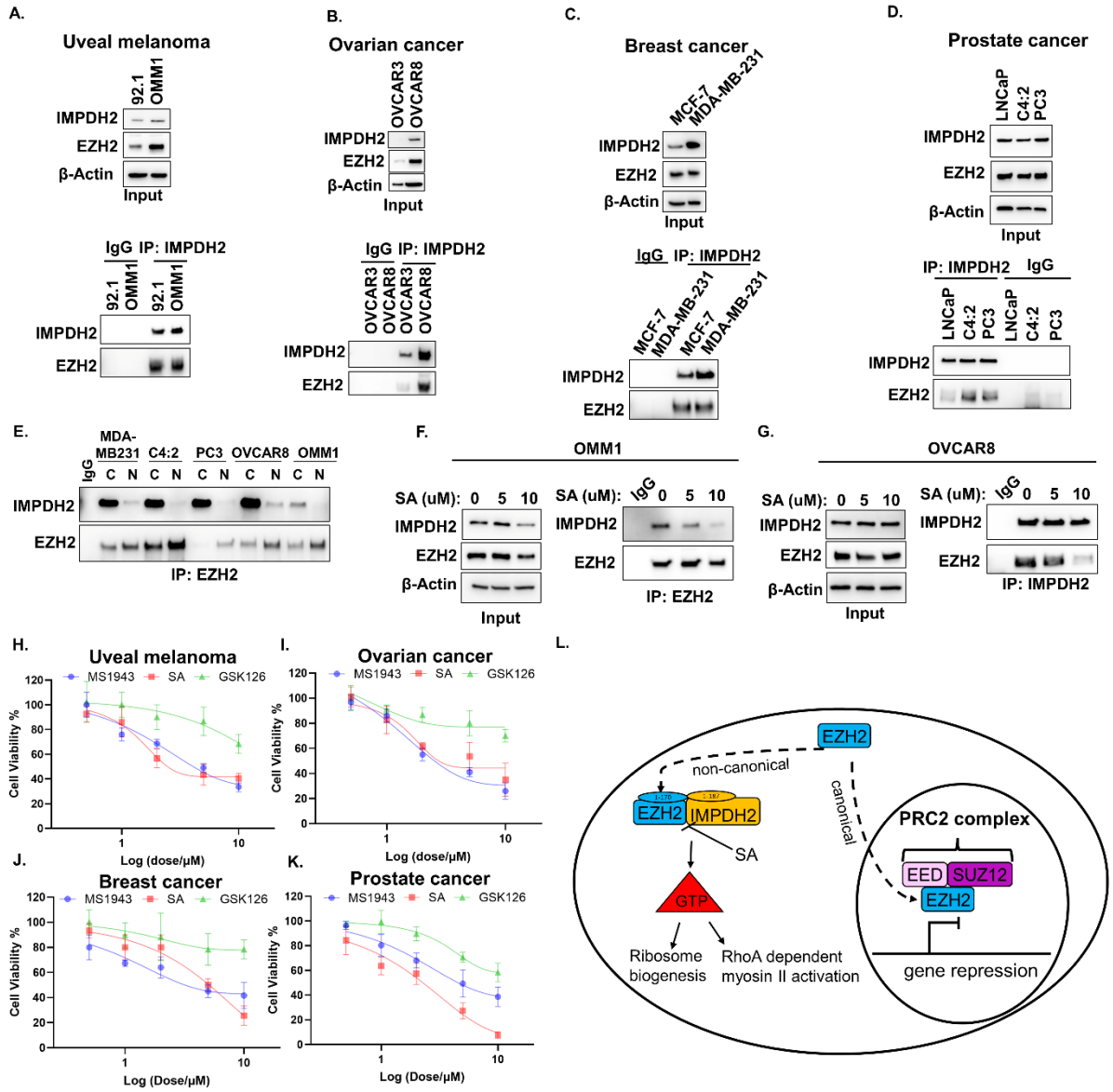
A.
Uveal melanoma
92.1
OMM1
IMPDH2
EZH2
β-Actin
Input
IgG IP: IMPDH2
92.1
OMM1
92.1
OMM1
IMPDH2
EZH2
B.
Ovarian cancer
OVCAR3
OVCAR8
IMPDH2
EZH2
β-Actin
Input
IgG IP: IMPDH2
OVCAR3
OVCAR8
OVCAR3
OVCAR8
IMPDH2
EZH2
C.
Breast cancer
MCF-7
MDA-MB-231
IMPDH2
EZH2
β-Actin
Input
IgG IP: IMPDH2
MCF-7
MDA-MB-231
MCF-7
MDA-MB-231
IMPDH2
EZH2
D.
Prostate cancer
LNCaP
C4:2
PC3
IMPDH2
EZH2
β-Actin
Input
IP: IMPDH2 IgG
LNCaP
C4:2
PC3
LNCaP
C4:2
PC3
IMPDH2
EZH2
E.
MDA-MB231
C4:2
PC3
OVCAR8
OMM1
IgG
C N C N C N C N C N
IMPDH2
EZH2
IP: EZH2
F.
OMM1
SA (uM): 0 5 10
IMPDH2
EZH2
β-Actin
Input
SA (uM): IgG 0 5 10
IMPDH2
EZH2
IP: EZH2
G.
OVCAR8
SA (uM): 0 5 10
IMPDH2
EZH2
β-Actin
Input
SA (uM): IgG 0 5 10
IMPDH2
EZH2
IP: IMPDH2
H.
Uveal melanoma
MS1943
SA
GSK126
Cell Viability %
Log (dose/μM)
I.
Ovarian cancer
MS1943
SA
GSK126
Cell Viability %
Log (dose/μM)
J.
Breast cancer
MS1943
SA
GSK126
Cell Viability %
Log (Dose/μM)
K.
Prostate cancer
MS1943
SA
GSK126
Cell Viability %
Log (Dose/μM)
L.
EZH2
non-canonical
canonical
EZH2
IMPDH2
SA
GTP
Ribosome biogenesis
RhoA dependent myosin II activation
PRC2 complex
EED
SUZ12
EZH2
gene repression

Supplemental Figures Legends

Figure S1. Pharmacological inhibition of EZH2 abundance, but not its activity reduces melanoma cell growth/ invasion and induces pigmentation. C006-M1 and IGR37 cells were treated with siEZH2, 2 μM DZNep, 2 μM GSK126, 2 μM EPZ6438 and scramble or DMSO (control) for 3 days prior to: (A, B) Western blot analysis of EZH2, H3K27me3, H3 and β-Actin protein level, (C, D) cell growth analysis done by Trypan Blue haemocytometer counting, (E) Matrigel-coated Boyden chamber invasion assay was assessed in pre-treated (3 days) cells seeded at 100,000 cells in 24-well plate coated with matrigel after incubation for 24h. (F) Invaded cell counts per well were done by CV staining. (G) Cell pigmentation was assessed by Fontana Masson staining. (H) Pigmented cell percentages were calculated per well. All experiments represent data from n=3 biological replicates. ns: non-significant, * $p< 0.01$, ** $p< 0.001$, *** $p< 0.0001$.

Figure S2. EZH2 has methyltransferase independent function in melanoma clonogenicity, invasion and pigmentation. (A) Western blot analysis of IGR37 cells showing EZH2 knockdown after lentiviral transduction with control shRNA (shControl) or 3′ UTR EZH2-targeting shRNA (shEZH2) and rescue with V5-tagged WT-EZH2 or methyltransferase deficient H689A-EZH2. (B) Clonogenicity assay of cells described in A. Representative images after crystal violet-stained wells were shown above bars and representative images of cell pellets were shown below bars. (C) Matrigel-coated Boyden chamber invasion assay of cells described in A. Representative images after crystal violet staining were shown above bars. (D). Western blot analysis of EZH2, V5, H3K27me3, H3 and β-Actin from A375 xenograft tumor lysates. Data for B, C are from three independent experiments and are presented as mean ±SD. **$p \leq 0.01$, ***$p \leq 0.005$.

Figure S3. EZH2 interacts with IMPDH2 and induces its tetramerization methyltransferase independently. (A) Western blot analysis of EZH2, IMPDH2 and β-Actin in C006-M1 (NRASQ61K), IGR37 (BRAFV600E), LM-MEL28: B4:F3 (BRAFV600E), C32 (BRAFV600E), SK-MEL28 (BRAFV600E), A375 (BRAFV600E), LM-MEL33 (BRAFV600E), LM-MEL45 (BRAFV600E), IGR39 (BRAFV600E) melanoma cells and normal human melanocytes (NHM). (B) Kaplan-Meier curves of overall survival of TCGA PanCancer Atlas cutaneous melanoma patients (n = 392

patients), stratified by IMPDH2 mRNA levels. (C) The interaction between endogenous EZH2 and IMPDH2 was determined in PDX tumor lysates by IP with anti-IMPDH2 and anti-EZH2 antibody followed by WB with anti-EZH2 and anti-IMPDH2 antibody. (D) A375 cells were treated with DMSO (control), 2 μM GSK126 or 2 μM EPZ6438 for 2 days prior to: (A) Western blot analysis of EZH2, H3K27me3, H3 and β-Actin (left) and interaction of EZH2/ IMPDH2 were shown by IP with anti-IMPDH2 antibody followed by WB with EZH2 antibody. (E) HA-tagged EZH2-WT and MYC/FLAG-tagged IMPDH2-WT were co-expressed in HEK293 cells. The interaction between overexpressed EZH2 and IMPDH2 was determined by immunoprecipitation with anti-HA antibody followed by western blotting with anti-Myc-tag antibody. (F) Co-immunofluorescence (Co-IF) staining with anti-EZH2 and anti-IMPDH2 antibodies. DAPI stains the nuclei. Scale bar: 20 μm (G) Western blot analysis of EZH2, V5, H3K27me3, H3 and β-Actin in A375 cells described in Figure 3F. (H) Tumor calipers of indicated A375 xenografts (n=7) at the end point. Data are presented as mean ±SD. ns: non-significant, * $p< 0.01$. (I) Cytosolic and nuclear Ezh2 phosphorylation sites and their percentages measured by LC-MS. Known kinases for the corresponding phospho-sites were also included on the last column of the table.?: Unknown kinases. (J) Western blot of of EZH2, V5, H3K27me3, H3 and β-Actin in A375 cells with control shRNA (shControl) or 3′ UTR EZH2-targeting shRNA and V5-EZH2-clone2. (K) Co-IF staining with anti-EZH2 and anti-IMPDH2 antibodies in C006-M1 cells treated with scramble control or siEZH2 for 3 days. DAPI stains the nuclei. Scale bar: 20 μm (L) IF staining with anti-V5 antibody in A375 cells harboring V5-IMPDH2 (1-187) that was treated with scramble control or siEZH2 for 3 days. DAPI stains the nuclei. Scale bar: 20 μm. (M) Cytosolic/Nuclear fractionation was done from A375 cells shown in J. Lamin A/C is nuclear, and β-Actin is cytosolic marker. The clusters of IMPDH2 tetramer were measured after cross-linking of B16-F10 cells (N) treated with or scramble control, siEzh2#1 orsiEzh2#2 for 3 days and of A375 cells shown in J (O).

Figure S4. Pharmacological or genetic inhibition of IMPDH2 reduces clonogenicity, invasion by p53 induction and ROCK-myosin II pathway activation. Time-dependent growth curves of A375 (A), C006-M1 (B), B4:F3 (C) cells upon 25 μM Ribavirin or DMSO (control); 3 μM MPA, or methanol (Control). (D) Clonogenicity assay of B16-F10 cells described in A. (E) Matrigel-coated Boyden chamber invasion assay of cells described in A, B. (F) Bright field images of cells

described in A, B, C. (G) B16-F10 cell senescence determined by β-gal staining (green). (H) Cell growth analysis done by Trypan Blue haemocytometer counting, (I) Western blot analysis of IMPDH2, β-Actin, p-MLC2 and MLC2 in A375 cells after treated with siIMPDH2#1, siIMPDH2#2 or scramble (control) for 3 days. (J, K) Western blot analysis of p53 and β-Actin in A375 cells with 0h, 4h, 8h 3 μM MPA treatment -/+ 100 μM guanosine. (L) Co-IF staining of A375 cells treated with 25 μM Ribavirin or DMSO (control); 3 μM MPA with anti-p53 (green) and anti-p21 (red) or anti-NCL (red), anti-FBL (green). DAPI stains the nuclei. Scale bar: 100 μm. (M) IF staining of A375 cells described in H with anti-p-MLC2 (green) and phalloidin (red). DAPI stains the nuclei. Scale bar: 20 μm.

Figure S5. EZH2 modulates ROCK-myosin II activity via Rho GTPase regulation in melanoma cells. (A) Western blot analysis of EZH2, IMPDH2, H3K27me3, H3, β-Actin, (B) Matrigel-coated Boyden chamber invasion assay in A375 cells with stable EZH2 knockdown (shEZH2) -/+ 100 μM guanosine for 3 days. (C) Western blot analysis of IMPDH2, EZH2 and β-Actin and (D) matrigel-coated Boyden chamber invasion assay in A375 cells with stable EZH2 knockdown and rescue with V5-tagged WT-EZH2 with scramble, si-IMPDH2#1, or si-IMPDH2#2 oligos and 100 μM guanosine addition. (E) IF staining with anti-NCL antibody in A375 cells with stable EZH2 knockdown (shEZH2) -/+ 100 μM guanosine for 3 days. (F) Western blot analysis of p53, EZH2, H3K27me3, H3, β-Actin (top) and qRT-PCR of *p53*, *MDM2*, *PUMA*, *CDKN2A* (bottom) in A375 cells with stable EZH2 knockdown. (G) p-MLC2 IF in A375 cells with stable EZH2 knockdown (shEZH2) -/+ 100 μM guanosine for 2 days. (H) Western blot analysis of p-MLC2, RhoA, EZH2, V5, β-Actin, H3K27me3 and H3 in A375 cells showing EZH2 knockdown shRNA (shControl) or 3′ UTR EZH2-targeting shRNA (shEZH2) and rescue with V5-tagged WT-EZH2 or methyltransferase deficient H689A-EZH2. (I) Western blot analysis of p-MLC2, MLC2, EZH2 and β-Actin in B16-F10 cells treated with scramble (control), siEzh2#1, or siEzh2#2 for 3 days. IF staining with anti-p-MLC2 antibody in B16-F10 (J) and A375 cells (K) treated with siEzh2#1, siEzh2#2, 2 μM DZNep, 2 μM GSK126, or 2 μM EPZ6438 for 2 days. DAPI stains the nuclei. Scale bar: 20 μm. % peripheral p-MLC2 positive cells were plotted below the images. (L) Nucleolar sizes were measured from HE stained xenograft samples obtained in Fig. 2F. Scale bar: 50 μm. (M) Co-IF with anti-DCT (melanocyte marker), anti-EZH2 and anti-IMPDH2 in normal human skin samples. Data for F, J, K and L are

from three independent experiments and are presented as mean ±SD. ns: non-significant, * p< 0.01, ** p< 0.001, *** p< 0.0001.

Figure S6. SA reduces EZH2/IMPDH2 interaction, IMPDH2 tetramerization/ nuclear translocation and attenuates the growth and invasion abilities of melanoma cells *in vitro*. (A) The interaction between endogenous EZH2 and IMPDH2 upon 16h SA treatment (DMSO, 5, 10, 20 μM) was determined in B16-F10 cells by Co-IP with anti-EZH2 antibody followed by WB with anti-EZH2 and anti-IMPDH2 antibody. The inputs were shown on the left. (B) The clusters of IMPDH2 tetramer were detected from cross-linked whole-cell extracts isolated from B16-F10 cells treated with indicated dose of SA for 16h. (D) Clonogenicity assay of A375 cells described in A. (E) Dose dependent cell growth curve of B16-F10 cells treated with the indicated doses of SA and -/+ 100 μM guanosine for 3 days. (F) Cell growth analysis of A375 cells with stable EZH2 knockdown and rescue with V5-tagged WT-EZH2 or methyltransferase deficient H689A-EZH2 followed by DMSO or 5 μM SA and 100 μM guanosine addition. (G) Time dependent sphere formation in 3D Matrigel (preventive). A375 and B16-F10 cells were grown in Matrigel for 4 d, 10 d and 14 d in the presence of either DMSO (control) or 5 μM SA. (H) Sphere formation in 3D Matrigel (preventive). B16-F10 cells were grown in Matrigel for 10 days in presence of either DMSO (control) or 10 μM SA and then the colonies were grown 7 more days without SA or DMSO and spheres were counted manually and presented in the graph (I). (J) Sphere formation in 3D Matrigel (therapeutic). B16-F10 cells were grown in Matrigel for 6 days in the absence of SA followed by 4d and 10d days with DMSO or 10 μM SA. Spheroid areas were measured by Image J program and presented in the graph (K). (L) The effect of SA on actomyosin contractility was measured in A375 cells treated with DMSO or 5 μM SA for 3 days with anti-p-MLC2 antibody (green) / Phalloidin (red) IF. DAPI stains the nuclei. Scale bar: 20 μm. Data for E, F, I, K and M are from three independent experiments and are presented as mean ±SD. ns: non-significant, * p< 0.01, *** p< 0.0001.

Figure S7. Cytosolic EZH2-IMPDH2 interaction is seen in uveal melanoma, breast, prostate, ovarian cancer, and SA attenuates IMPDH2 tetramerization. EZH2 and IMPDH2 interaction was shown by IP with anti-EZH2 antibody followed by WB with anti-EZH2 and anti-IMPDH2 antibody in (A) uveal melanoma, (B) ovarian cancer, (C) breast cancer and (D) prostate cancer cell lines. (E) Cytosolic/Nuclear

fractionation was done for OMM1, OVCAR8, MDA-MD231 and C4:2 cells followed by IP with anti-IMPDH2 antibody followed by western blotting with anti-EZH2 and anti-IMPDH2 antibody. Lamin A/C is nuclear, and β-Actin is cytosolic marker. Inputs were shown above the IP blot. The effect of SA on EZH2 and IMPDH2 interaction was shown by Co-IP coupled WB in (F) MDA-MB-231 and (G) PC3 cells. The clusters of IMPDH2 tetramer were detected from cross-linked whole-cell extracts isolated from (H) OMM1, (I) OVCAR8, (J) MDA-MB-231 and (K) PC3 cells treated with the indicated dose of SA for 16h.

Figure S1.

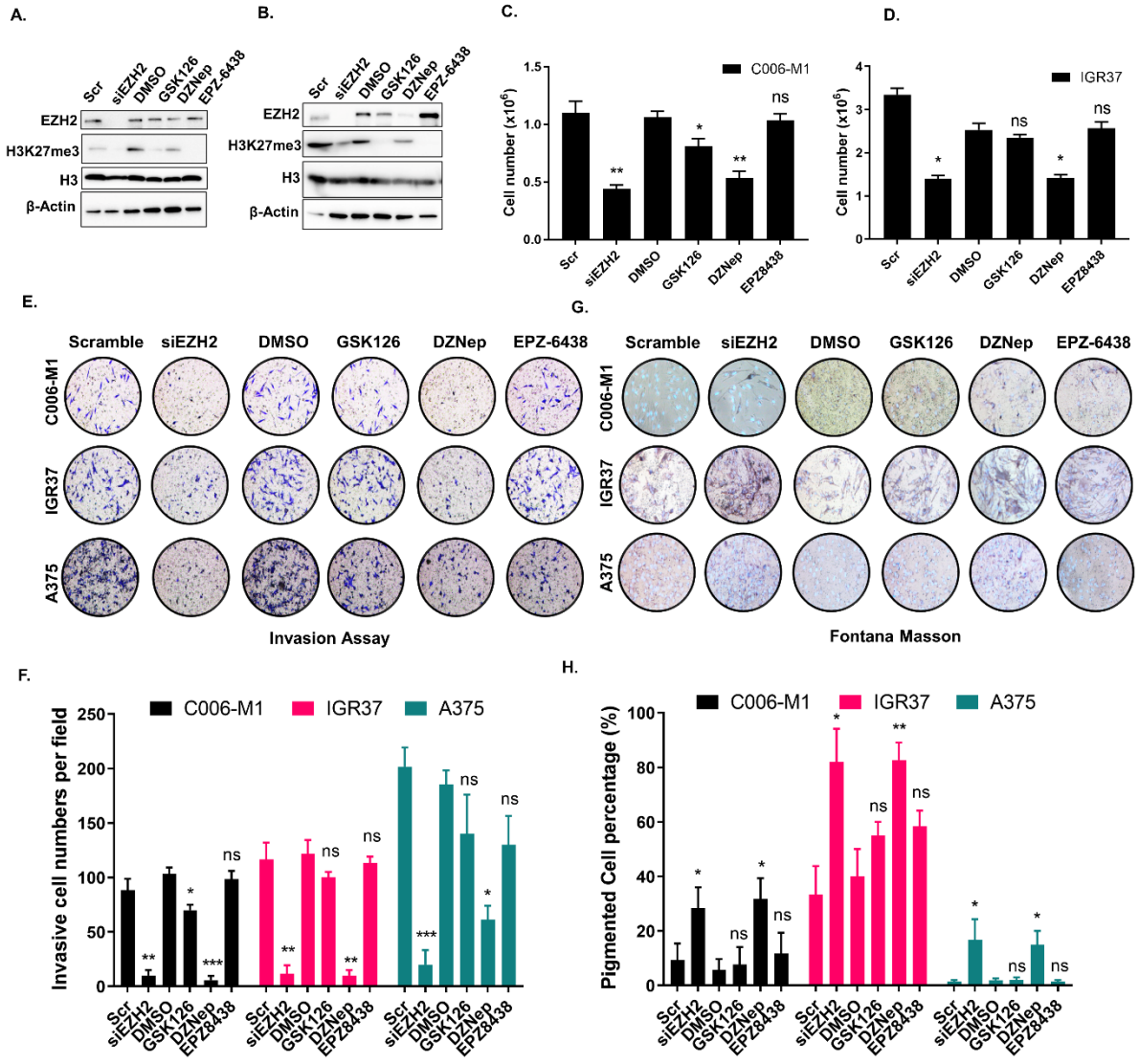
A.
Scr
siEZH2
DMSO
GSK126
DZNep
EPZ-6438
EZH2
H3K27me3
H3
β-Actin
B.
C.
C006-M1
Cell number (x10^6)
D.
IGR37
E.
Scramble
siEZH2
DMSO
GSK126
DZNep
EPZ-6438
C006-M1
IGR37
A375
Invasion Assay
G.
Fontana Masson
F.
Invasive cell numbers per field
H.
Pigmented Cell percentage (%)

Figure S2.

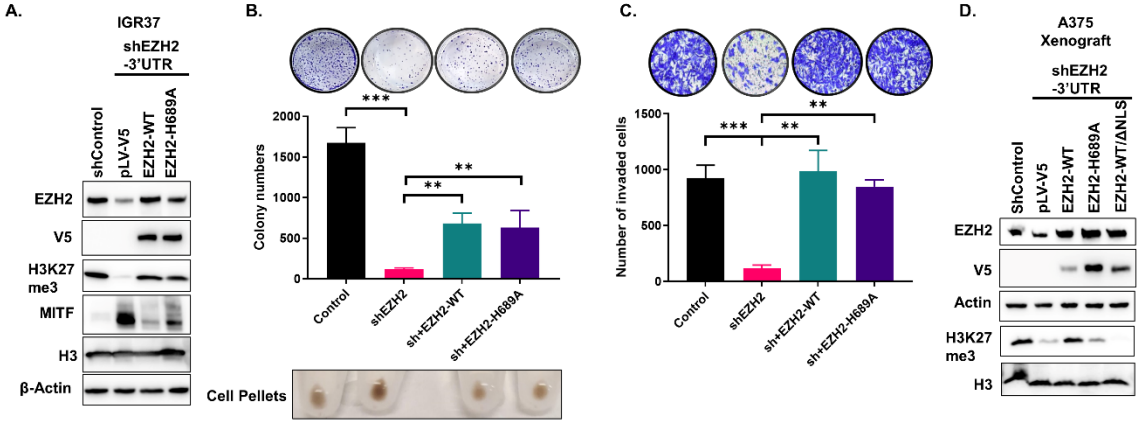
A.
IGR37
shEZH2
-3'UTR
shControl
pLV-V5
EZH2-WT
EZH2-H689A
EZH2
V5
H3K27
me3
MITF
H3
β-Actin
B.
Colony numbers
2000
1500
1000
500
0
***
**
**
Control
shEZH2
sh+EZH2-WT
sh+EZH2-H689A
Cell Pellets
C.
Number of invaded cells
1500
1000
500
0
***
**
**
Control
shEZH2
sh+EZH2-WT
sh+EZH2-H689A
D.
A375
Xenograft
shEZH2
-3'UTR
ShControl
pLV-V5
EZH2-WT
EZH2-H689A
EZH2-WT/ΔNLS
EZH2
V5
Actin
H3K27
me3
H3

Figure S3.

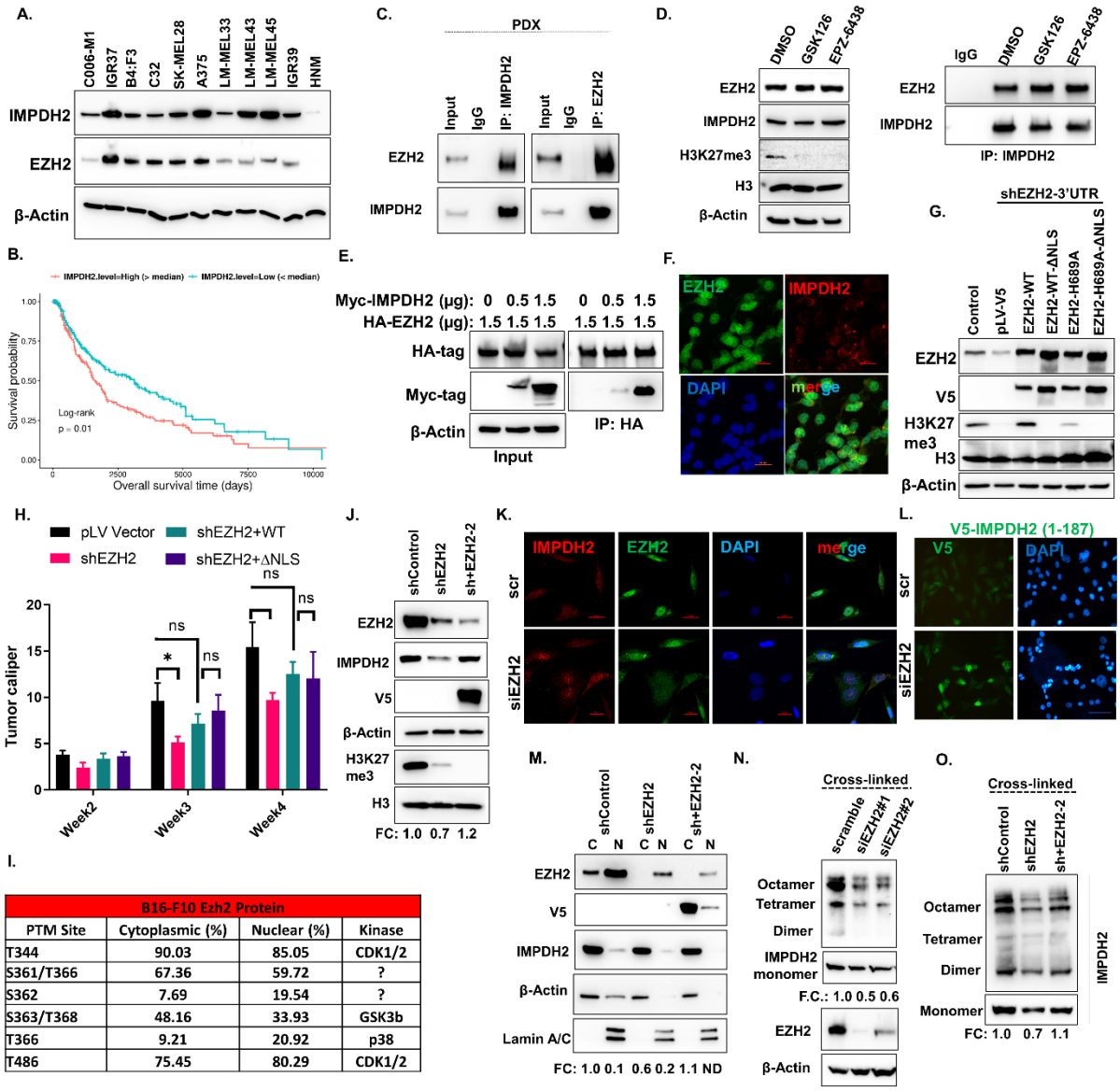

I.

B16-F10 Ezh2 Protein			
PTM Site	Cytoplasmic (%)	Nuclear (%)	Kinase
T344	90.03	85.05	CDK1/2
S361/T366	67.36	59.72	?
S362	7.69	19.54	?
S363/T368	48.16	33.93	GSK3b
T366	9.21	20.92	p38
T486	75.45	80.29	CDK1/2

Figure S4.

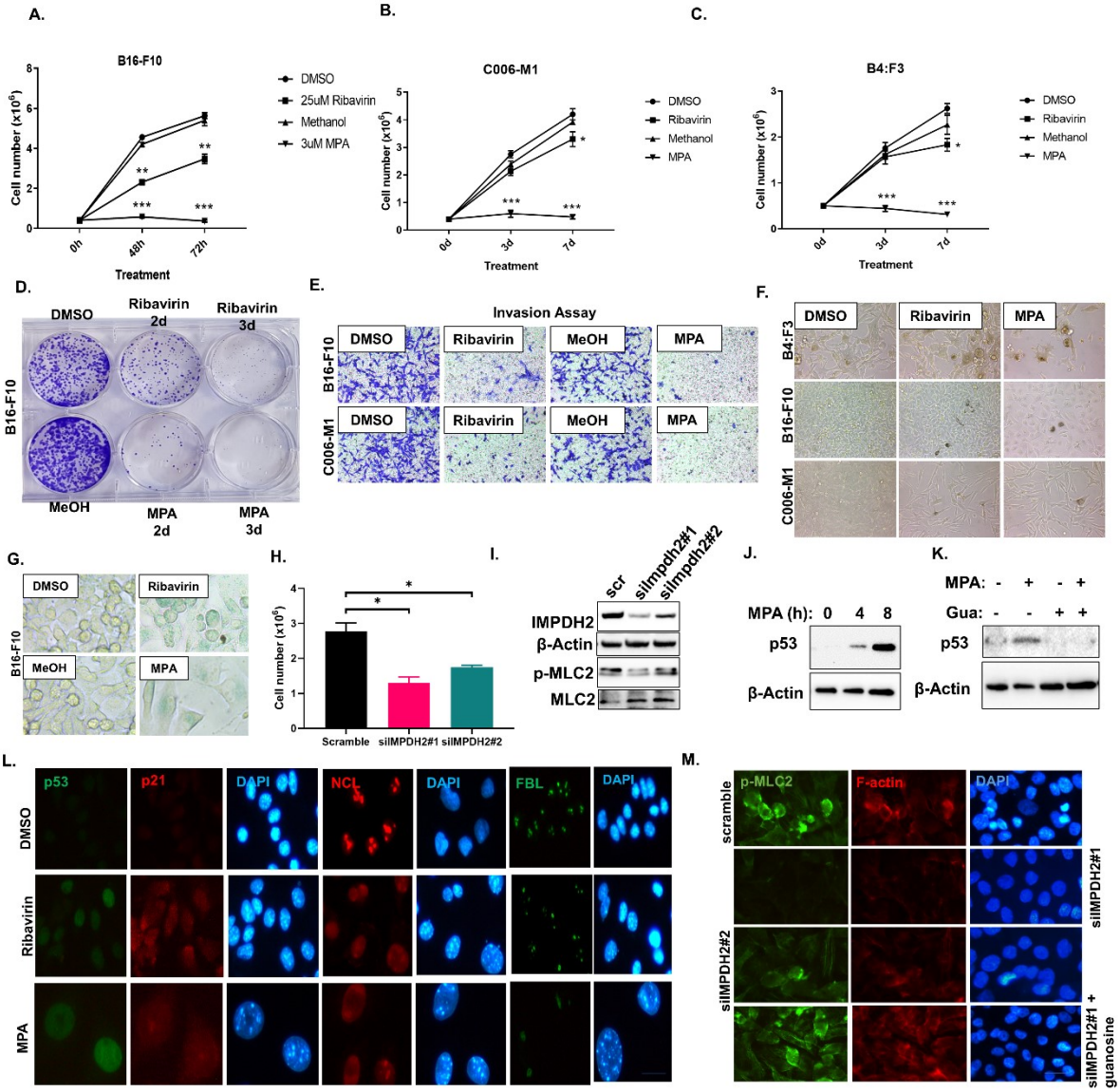
A.
B16-F10
Cell number (x10^6)
Treatment
0h
48h
72h
DMSO
25uM Ribavirin
Methanol
3uM MPA
B.
C006-M1
Cell number (x10^5)
Treatment
0d
3d
7d
DMSO
Ribavirin
Methanol
MPA
C.
B4:F3
Cell number (x10^6)
Treatment
0d
3d
7d
DMSO
Ribavirin
Methanol
MPA
D.
B16-F10
DMSO
Ribavirin 2d
Ribavirin 3d
MeOH
MPA 2d
MPA 3d
E.
Invasion Assay
B16-F10
C006-M1
DMSO
Ribavirin
MeOH
MPA
F.
B4:F3
B16-F10
C006-M1
DMSO
Ribavirin
MPA
G.
B16-F10
DMSO
Ribavirin
MeOH
MPA
H.
Cell number (x10^6)
Scramble
siIMPDH2#1
siIMPDH2#2
I.
scr
siImpdh2#1
siImpdh2#2
IMPDH2
β-Actin
p-MLC2
MLC2
J.
MPA (h): 0 4 8
p53
β-Actin
K.
MPA: - + - +
Gua: - - + +
p53
β-Actin
L.
p53
p21
DAPI
NCL
DAPI
FBL
DAPI
DMSO
Ribavirin
MPA
M.
p-MLC2
F-actin
DAPI
scramble
siIMPDH2#1
siIMPDH2#2
siIMPDH2#1 + guanosine

Figure S5.

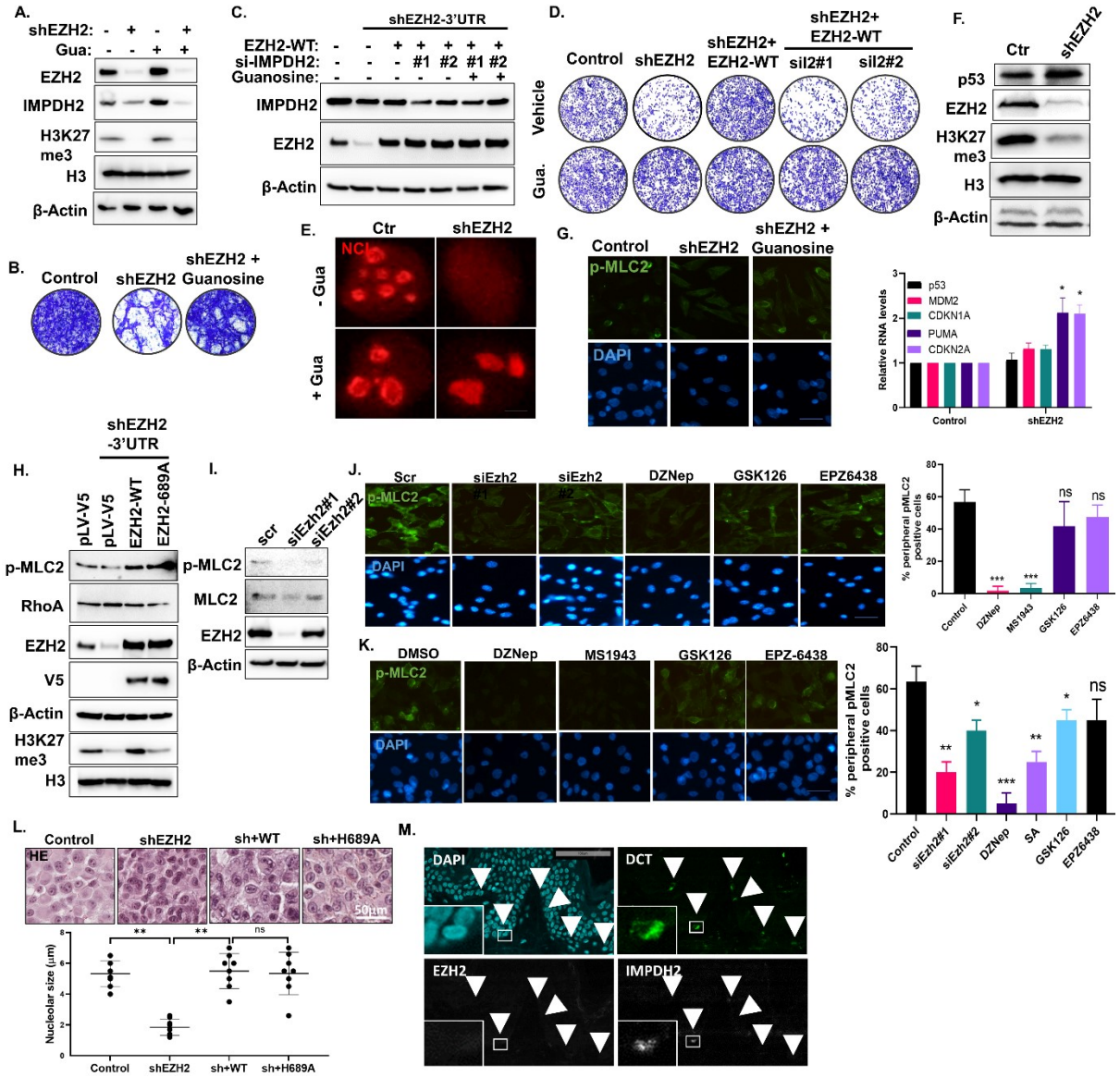
A.
shEZH2: - + - +
Gua: - - + +
EZH2
IMPDH2
H3K27 me3
H3
β-Actin
B.
Control
shEZH2
shEZH2 + Guanosine
C.
shEZH2-3'UTR
EZH2-WT: - - + + + + +
si-IMPDH2: - - - #1 #2 #1 #2
Guanosine: - - - - - + +
IMPDH2
EZH2
β-Actin
D.
Control
shEZH2
shEZH2+ EZH2-WT
shEZH2+ EZH2-WT
siI2#1
siI2#2
Vehicle
Gua.
E.
Ctr
shEZH2
NCI
- Gua
+ Gua
F.
Ctr
shEZH2
p53
EZH2
H3K27 me3
H3
β-Actin
G.
Control
shEZH2
shEZH2 + Guanosine
p-MLC2
DAPI
p53
MDM2
CDKN1A
PUMA
CDKN2A
Relative RNA levels
Control
shEZH2
H.
shEZH2 -3'UTR
pLV-V5
pLV-V5
EZH2-WT
EZH2-689A
p-MLC2
RhoA
EZH2
V5
β-Actin
H3K27 me3
H3
I.
scr
siEzh2#1
siEzh2#2
p-MLC2
MLC2
EZH2
β-Actin
J.
Scr
siEzh2 #1
siEzh2 #2
DZNep
GSK126
EPZ6438
p-MLC2
DAPI
% peripheral pMLC2 positive cells
Control
DZNep
MS1943
GSK126
EPZ6438
K.
DMSO
DZNep
MS1943
GSK126
EPZ-6438
p-MLC2
DAPI
% peripheral pMLC2 positive cells
Control
siEzh2#1
siEzh2#2
DZNep
SA
GSK126
EPZ6438
L.
Control
shEZH2
sh+WT
sh+H689A
HE
50µm
Nucleolar size (µm)
Control
shEZH2
sh+WT
sh+H689A
M.
DAPI
DCT
EZH2
IMPDH2

Figure S6.

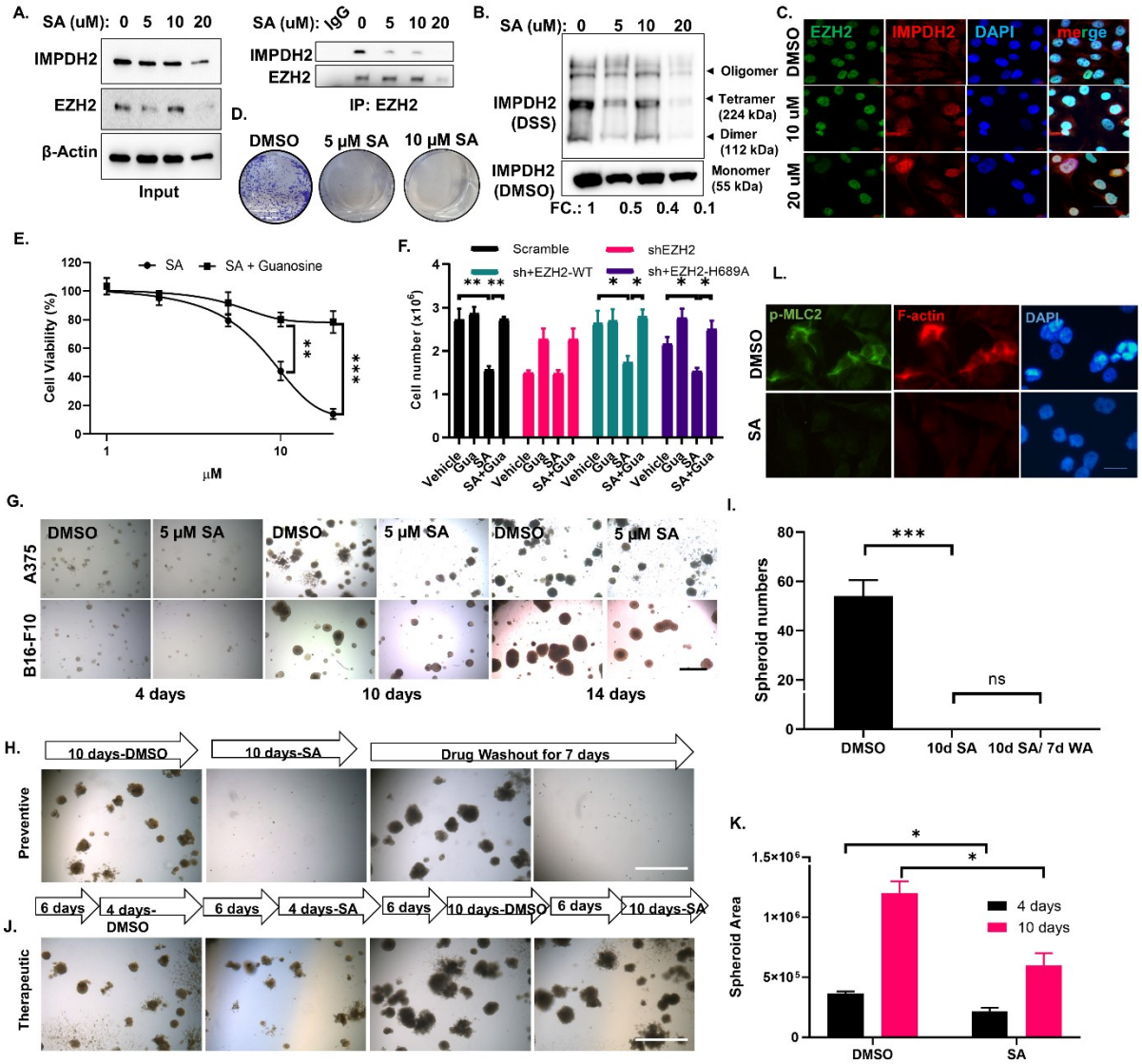
A.
SA (uM): 0 5 10 20
IMPDH2
EZH2
β-Actin
Input
SA (uM): IgG 0 5 10 20
IMPDH2
EZH2
IP: EZH2
B.
SA (uM): 0 5 10 20
IMPDH2 (DSS)
IMPDH2 (DMSO)
Oligomer
Tetramer (224 kDa)
Dimer (112 kDa)
Monomer (55 kDa)
FC.: 1 0.5 0.4 0.1
C.
EZH2
IMPDH2
DAPI
merge
DMSO
10 uM
20 uM
D.
DMSO
5 μM SA
10 μM SA
E.
SA
SA + Guanosine
Cell Viability (%)
μM
F.
Scramble
shEZH2
sh+EZH2-WT
sh+EZH2-H689A
Cell number (x10^6)
Vehicle
Gua
SA
SA+Gua
L.
p-MLC2
F-actin
DAPI
DMSO
SA
G.
A375
B16-F10
DMSO
5 μM SA
4 days
10 days
14 days
I.
Spheroid numbers
***
ns
DMSO
10d SA
10d SA/ 7d WA
H.
10 days-DMSO
10 days-SA
Drug Washout for 7 days
Preventive
J.
6 days
4 days-DMSO
4 days-SA
10 days-DMSO
10 days-SA
Therapeutic
K.
Spheroid Area
4 days
10 days
DMSO
SA

Figure S7.

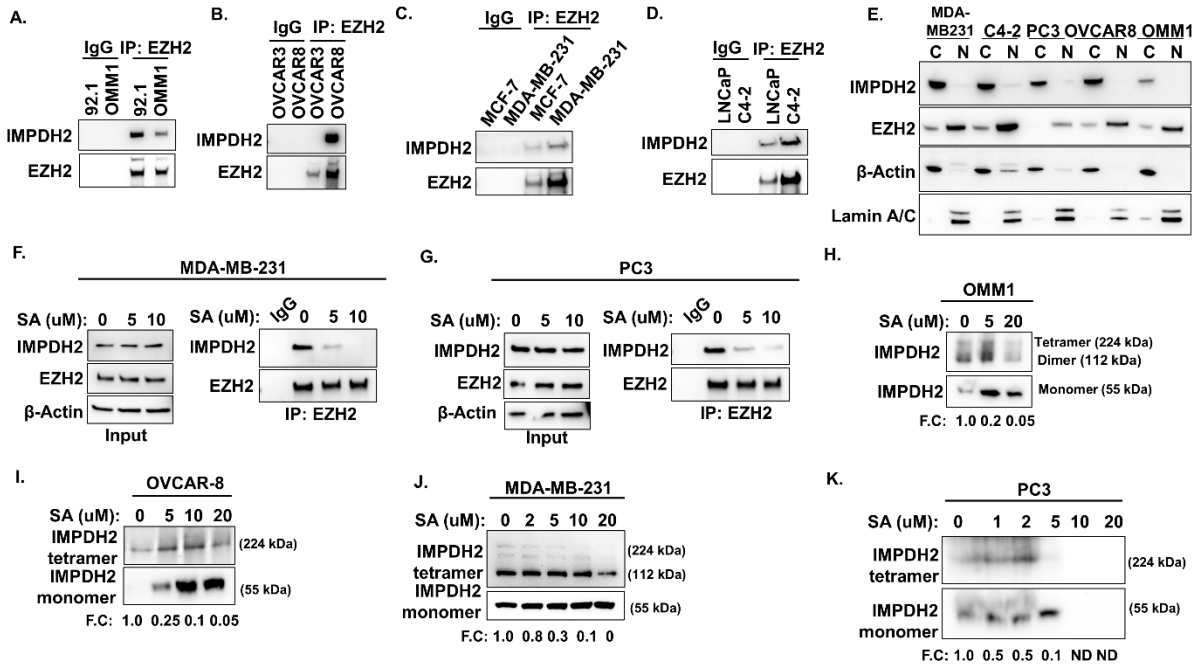
A.
IgG IP: EZH2
92.1 OMM1 92.1 OMM1
IMPDH2
EZH2
B.
IgG IP: EZH2
OVCAR3 OVCAR8 OVCAR3 OVCAR8
IMPDH2
EZH2
C.
IgG IP: EZH2
MCF-7 MDA-MB-231 MCF-7 MDA-MB-231
IMPDH2
EZH2
D.
IgG IP: EZH2
LNCaP C4-2 LNCaP C4-2
IMPDH2
EZH2
E.
MDA-MB231 C4-2 PC3 OVCAR8 OMM1
C N C N C N C N C N
IMPDH2
EZH2
β-Actin
Lamin A/C
F.
MDA-MB-231
SA (uM): 0 5 10
IMPDH2
EZH2
β-Actin
Input
SA (uM): IgG 0 5 10
IMPDH2
EZH2
IP: EZH2
G.
PC3
SA (uM): 0 5 10
IMPDH2
EZH2
β-Actin
Input
SA (uM): IgG 0 5 10
IMPDH2
EZH2
IP: EZH2
H.
OMM1
SA (uM): 0 5 20
IMPDH2
Tetramer (224 kDa)
Dimer (112 kDa)
IMPDH2
Monomer (55 kDa)
F.C: 1.0 0.2 0.05
I.
OVCAR-8
SA (uM): 0 5 10 20
IMPDH2 tetramer
(224 kDa)
IMPDH2 monomer
(55 kDa)
F.C: 1.0 0.25 0.1 0.05
J.
MDA-MB-231
SA (uM): 0 2 5 10 20
IMPDH2 tetramer
(224 kDa)
(112 kDa)
IMPDH2 monomer
(55 kDa)
F.C: 1.0 0.8 0.3 0.1 0
K.
PC3
SA (uM): 0 1 2 5 10 20
IMPDH2 tetramer
(224 kDa)
IMPDH2 monomer
(55 kDa)
F.C: 1.0 0.5 0.5 0.1 ND ND